Article

Cell Reports

Rad53-Mediated Regulation of Rrm3 and Pif1 DNA Helicases Contributes to Prevention of Aberrant Fork Transitions under Replication Stress

Graphical Abstract

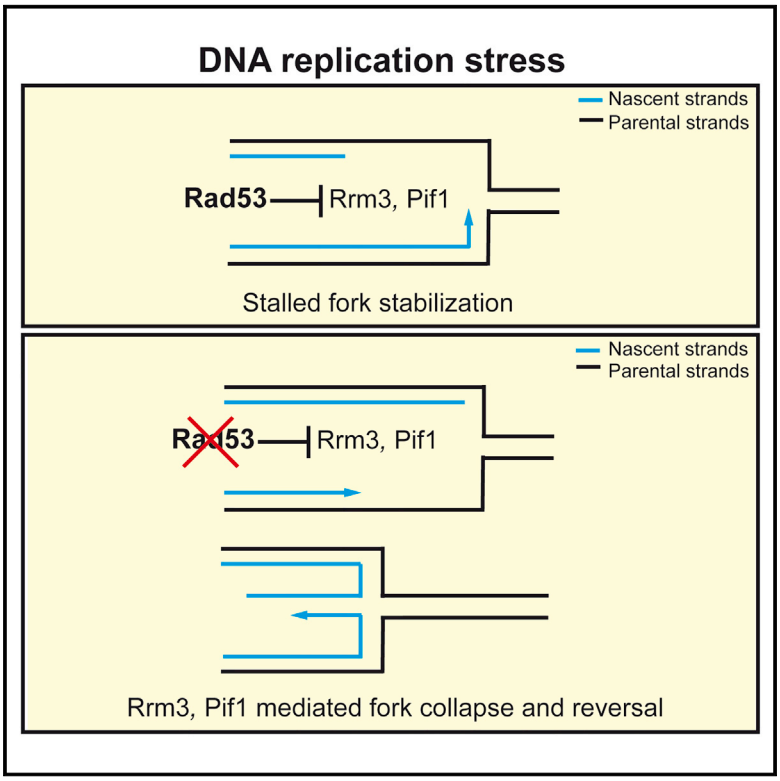

Authors

Silvia Emma Rossi, Arta Ajazi, Walter Carotenuto, Marco Foiani, Michele Giannattasio

Correspondence

marco.foiani@ifom.eu (M.F.), michele.giannattasio@ifom.eu (M.G.)

In Brief

Rossi et al. show that the DNA helicases Rrm3 and Pif1 associate with stalled DNA replication forks and undergo Rad53-mediated phosphorylation. The authors suggest that Rrm3 and Pif1 promote fork reversal, fork stalling, and chromosome fragility in *rad53* defective cells under replication stress.

Highlights

- Rrm3 and Pif1 promote fork reversal and ssDNA gaps at stalled forks in *rad53* cells
- Rrm3 and Pif1 associate with stalled DNA replication forks
- Rad53 phosphorylates Rrm3 and Pif1 at stalled forks
- Rrm3 and Pif1 promote chromosome fragility in hydroxyurea-treated *rad53* cells

Accession Numbers

GSE68214

Rossi et al., 2015, Cell Reports *13*, 80–92
October 6, 2015
http://dx.doi.org/10.1016/j.celrep.2015.08.073

OPEN ACCESS
CellPress

Cell Reports
Article

Rad53-Mediated Regulation of Rrm3 and Pif1 DNA Helicases Contributes to Prevention of Aberrant Fork Transitions under Replication Stress

Silvia Emma Rossi,[1,2] Arta Ajazi,[1,2] Walter Carotenuto,[1] Marco Foiani,[1,2,*] and Michele Giannattasio[1,2,*]
[1]IFOM (Fondazione Istituto FIRC di Oncologia Molecolare), Via Adamello 16, 20139 Milan, Italy
[2]Dipartimento di Bioscienze, Università degli Studi di Milano, Via Celoria 26, 20133 Milan, Italy
*Correspondence: marco.foiani@ifom.eu (M.F.), michele.giannattasio@ifom.eu (M.G.)
http://dx.doi.org/10.1016/j.celrep.2015.08.073

SUMMARY

Replication stress activates the Mec1^{ATR} and Rad53 kinases. Rad53 phosphorylates nuclear pores to counteract gene gating, thus preventing aberrant transitions at forks approaching transcribed genes. Here, we show that Rrm3 and Pif1, DNA helicases assisting fork progression across pausing sites, are detrimental in *rad53* mutants experiencing replication stress. Rrm3 and Pif1 ablations rescue cell lethality, chromosome fragmentation, replisome-fork dissociation, fork reversal, and processing in *rad53* cells. Through phosphorylation, Rad53 regulates Rrm3 and Pif1; phospho-mimicking *rrm3* mutants ameliorate *rad53* phenotypes following replication stress without affecting replication across pausing elements under normal conditions. Hence, the Mec1-Rad53 axis protects fork stability by regulating nuclear pores and DNA helicases. We propose that following replication stress, forks stall in an asymmetric conformation by inhibiting Rrm3 and Pif1, thus impeding lagging strand extension and preventing fork reversal; conversely, under unperturbed conditions, the peculiar conformation of forks encountering pausing sites would depend on active Rrm3 and Pif1.

INTRODUCTION

Replication forks pause at specific sites under unperturbed conditions (Deshpande and Newlon, 1996). Fork stalling occurs in response to intra-S DNA damage or DNA synthesis inhibition. Hydroxyurea (HU) causes deoxi-nucleotides triphosphate (dNTPs) deprivation (Krakoff et al., 1968), fork stalling, and activation of the Mec1^{ATR} and Rad53 kinases that protect stalled fork stability (Branzei and Foiani, 2009). The *mec1* and *rad53* mutants exhibit accumulation of single-stranded DNA (ssDNA) and chromosome fragmentation under replication stress (Cha and Kleckner, 2002; Feng et al., 2006; Hashash et al., 2011). *rad53* mutants treated with HU undergo fork collapse and accumulation of hemi-replicated, gapped, and reversed forks (Sogo et al., 2002). The Mec1-Rad53 axis has also been implicated in controlling replisome-fork association (Cobb et al., 2005; Lucca et al., 2004) in response to replication stress, although this aspect has been challenged (De Piccoli et al., 2012). Following HU treatments, human Chk1 (with functionally similar to Rad53) prevents aberrant origin firing, apoptosis, and fork processing by the Mus81/Eme1 nuclease and the Rqh1 DNA helicase, which promote chromosome breakages (Doe et al., 2002; Forment et al., 2011; Syljuåsen et al., 2005). In *S. pombe,* Cds1^{Rad53} prevents unscheduled Mus81/Eme1-mediated fork processing (Froget et al., 2008) and targets Dna2 to counteract fork reversal (Hu et al., 2012). Downregulation of *ATR* under replication stress causes fragile site expression (Casper et al., 2002) and chromosome fragmentation through a *SMARCAL1/SLX4*-dependent process (Couch et al., 2013). It has been found that ATR prevents RPA exhaustion under replication stress to avoid catastrophic events at forks (Toledo et al., 2013). While in the yeasts *S. cerevisiae* and *S. pombe* fork reversal has been related to pathological events (Hu et al., 2012; Lopes et al., 2006), studies in mammalian cell lines have suggested that reversed forks may assist replication restart (Berti et al., 2013; Zellweger et al., 2015). The protective role of Rad53 against replication stress relies on its serine/threonine kinase activity (Sun et al., 1996). Following HU treatment, Rad53 increases the dNTP pool by phosphorylating Sml1 and Crt1 (Huang et al., 1998; Zhao and Rothstein, 2002), prevents late origin firing through the phosphorylation of Sld3 and Dbf4 (Zegerman and Diffley, 2010), and counteracts dangerous topological transitions at transcribed loci by phosphorylating the Mlp1 nucleoporin (Bermejo et al., 2011). Pif1 and Rrm3 in *S. cerevisiae* and Pfh1 in *S. pombe* are 5′-to-3′-directed DNA helicases, which assist DNA replication fork progression in unperturbed conditions across different pausing elements, such as *rDNA*, *tRNA*, telomeres, centromeres, *HML/HMR* loci, inactive origins, RNA polymerase II (Pol II)-transcribed genes, and G quadruplexes (Bochman et al., 2010; Ivessa et al., 2000, 2003; Paeschke et al., 2011, 2013; Sabouri et al., 2012). Rrm3 removes bulky non-nucleosomal DNA-protein complexes ahead of replication forks while it seems less essential for fork progression across pausing sites containing RNA Pol II-transcribed elements (Azvolinsky et al., 2009; Ivessa et al., 2003). Pif1 unwinds problematic DNA structures (Paeschke et al., 2011, 2013). Pfh1 assists fork progression across pausing

elements containing non-nucleosomal DNA-protein complexes and RNA polymerase I-, II-, and III-transcribed elements (Sabouri et al., 2012). Rrm3 moves with the fork in unperturbed conditions and interacts with DNA polymerase ε (Pol ε), PCNA, and Orc5 (Azvolinsky et al., 2006; Matsuda et al., 2007; Schmidt et al., 2002). Pif1 unwinds Okazaki fragments, which cannot be processed by the *RAD27/FEN1* endonuclease in the so-called alternative pathway of Okazaki fragment processing, which involves Dna2 (Budd et al., 2006; Pike et al., 2009, 2010; Rossi et al., 2008). Pif1 generates lethal overloads of toxic long 5′ DNA flaps on the lagging strand in *dna2* mutants (Budd et al., 2006) and is responsible for unscheduled unwinding activities of uncapped telomeres in *cdc13* mutants (Dewar and Lydall, 2010).

Here, we show that Rrm3 and Pif1 associate with stalled forks and undergo Rad53-dependent hyper-phosphorylation under replication stress. Their ablations suppress fork collapse, chromosome fragmentation, and cell lethality in *rad53* cells under replication stress. Phospho-mimicking *rrm3* alleles alleviate the HU sensitivity of *rad53* mutants while they are proficient in assisting fork progression under normal conditions. We propose that Rad53 inhibits Rrm3 and Pif1 by phosphorylation in response to replication stress to prevent fork reversal, chromosome fragmentation, and genome instability.

RESULTS

Rrm3 and Pif1 Associate with Forks following Replication Stress

We used chromatin immunoprecipitation on chip (ChIP-chip) (Bermejo et al., 2009a, 2009b), to investigate whether Rrm3 and Pif1 associated with forks in the presence of HU in a Rad53-dependent manner. We used ssDNA-bromodeoxyuridine immunoprecipitation on chip (BrdU-chip) to visualize DNA synthesis at the genome level (Bermejo et al., 2009b; Katou et al., 2003). All strains used in this study are listed in Table S1.

Wild-type (WT) and *rad53-K227A* strains carrying Rrm3-Myc or Polα-Myc (Figure 1A) and *sml1Δ* and *sml1Δ rad53Δ* strains carrying Pif1-FLAG or Polα-FLAG (Figures 1B and S1A) were released from G1 into 150 mM HU for 90 min. The Polα clusters co-localized with the boundaries of the BrdU peaks, generated by forks emanating from active origins (Figures 1A and 1B). The average binding signals of Polα clusters at 141 early *ARS*s (Figure 1C) showed a bimodal distribution in WT cells due to forks moving away from the origin point; conversely, in *rad53* cells, the binding signals were more centered on the origin point due to impaired fork progression. We consistently noticed that the Polα signal intensity was reduced in *rad53* mutants compared to WT cells (Figures 1A–1C and S1B). We confirmed this observation by quantitative ChIP-qPCR (Figure 1D). This observation is consistent with what was previously shown (Lucca et al., 2004) and likely reflects the extensive fork collapse, typical of HU-treated *rad53* cells (Lopes et al., 2001). Checkpoint mutants exhibit unscheduled firing of late and dormant origins (Santocanale and Diffley, 1998; Shirahige et al., 1998). Specifically, in *rad53* mutants, late and dormant origins exhibited Polα clusters, which co-localized with Rrm3 and Pif1 binding sites (Figures 1A, 1B. and S1C). The average signals of Rrm3 and Pif1 clusters at the 141 early *ARS*s showed that both proteins paralleled the Polα distributions in WT and *rad53* cells (Figure 1C).

However, although the intensity of the Rrm3 clusters resembled the one of Polα in *rad53* mutants, the intensity of Pif1 clusters was higher in the absence of Rad53. These observations were confirmed by quantitative ChIP-qPCR (Figure 1D) and suggest that Rrm3 progressively dissociates from the forks and that *rad53* mutants accumulate Pif1-dependent replication intermediates at stalled forks. The Rrm3 and Pif1 distributions paralleled the ones of Polα at those dormant and late origins, which specifically fired in *rad53* cells (Figures 1A, 1B, and S1C).

We analyzed the Polα-Flag, Rrm3-Myc, and Pif1-Flag genomic clusters in WT and *rad53* mutants treated with 25 mM HU (Figure 2A). Under these conditions, forks in *rad53* cells do not collapse soon after origin firing but rather progress further, until they encounter replication risk elements (such as replication slow zones [RSZs]), where they promote fragile site expression (Cha and Kleckner, 2002; Hashash et al., 2011). The *sml1Δ* and *sml1Δ rad53Δ* strains were released from G1 into HU for 45 min (Figure 2A). As expected, the BrdU clusters extended outside the *ARS305* locus in both *sml1Δ* and *sml1Δ rad53Δ* mutants, but their progression was impaired in *rad53* mutants. Moreover, the dormant origins *ARS313* and *ARS314* specifically fired in *rad53* but not in WT cells (Figure 2A). While in *sml1* cells the Rrm3-Myc, Pif1-Flag, and Polα-Flag clusters, originating from the right forks of *ARS305*, almost completely passed through the HindIII-*YCL044C* flanking locus (positioned around 5 kb from the *ARS305* origin), in *sml1Δ rad53Δ*, most forks were still localized within the *YCL044C*-containing fragment (Figure 2A). Hence, Rrm3 and Pif1 remained associated to the slow-moving forks, typical of *rad53* mutants treated with low HU concentrations.

Altogether, these observations suggest that, under replication stress, Rrm3 and Pif1 likely associate with the replisome, the fork, or both and that this association is not lost in *rad53* mutants.

Fork Abnormalities in *rad53* Mutants Depend on Rrm3 and Pif1

We investigated whether Rrm3 and Pif1 influenced the fate of the forks in *rad53* cells following replication stress. We ablated *RRM3* and the *PIF1* nuclear form (by using the *pif1-m2* allele, which retains the mitochondrial function of Pif1) (Schulz and Zakian, 1994), in *sml1Δ* and *sml1Δ rad53Δ* strains. The two sets of strains—*sml1Δ*, *sml1Δ pif1-m2*, *sml1Δ rrm3Δ*, *sml1Δ pif1-m2 rrm3Δ* and *sml1Δ rad53Δ*, *sml1Δ rad53Δ pif1-m2*, *sml1Δ rad53Δ rrm3Δ*, *sml1Δ rad53Δ pif1-m2 rrm3Δ*—were released from G1 into 25 mM HU for 90 min and analyzed by neutral-neutral 2D gels after in vivo chromatin psoralen crosslinking (Liberi et al., 2006) (Figure 2B). Under these conditions, the *sml1* set of strains reached near-2C DNA content even in the presence of HU. Conversely, within the *sml1 rad53* set of strains, only *sml1Δ rad53Δ pif1-m2 rrm3Δ* cells almost completed replication by 90 min (Figure 2B, red arrow). When we analyzed by 2D gel in the *sml1* strains the *YCL044C* locus 90 min after G1 release, we failed to visualize replication intermediates, as most forks had already passed through that genomic fragment (Figures 2A and 2B). Conversely, *sml1Δ rad53Δ* cells exhibited a strong

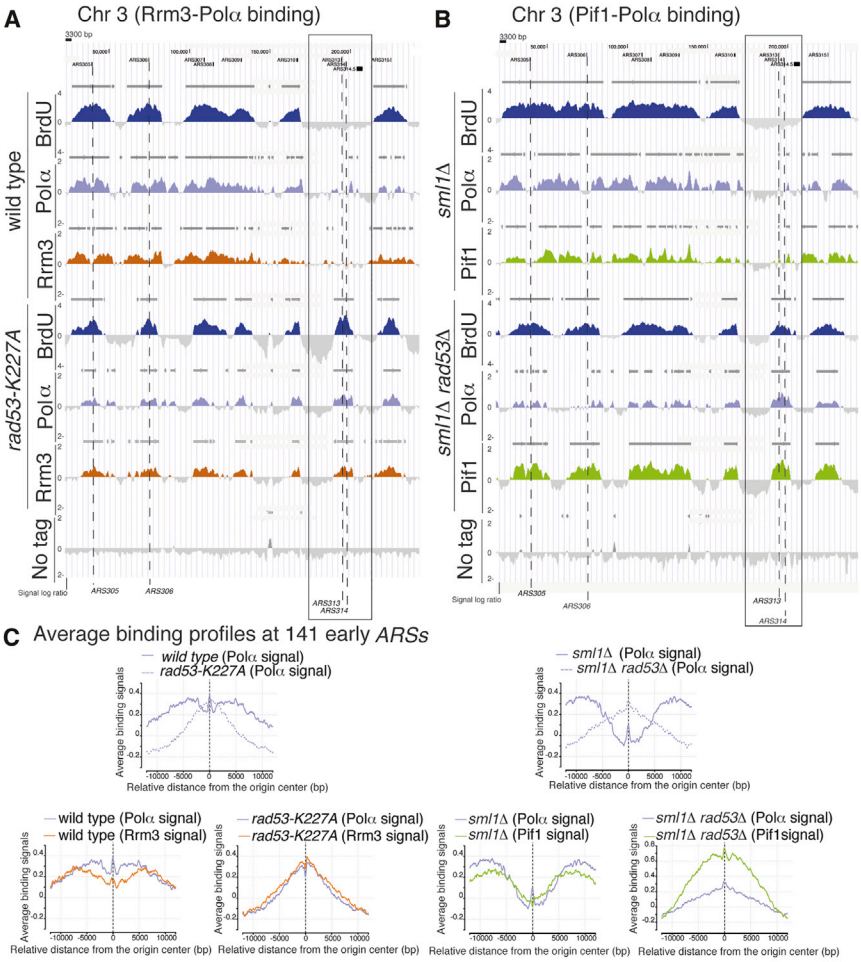

Figure 1. Rrm3 and Pif1 Associate with the Forks under Replication Stress

(A) Rrm3-13Myc (red) and Polα-9Myc (light blue) binding profiles were determined in strains CY11360, CY12425, CY12927, and CY12698 released from G1 into 150 mM HU for 90 min. Dashed black lines indicate early (*ARS305* and *ARS306*) and dormant (*ARS313* and *ARS314*) origins. Dark gray horizontal bars above the binding profiles indicate the significant binding clusters. A black scale bar indicates the distance corresponding to 3,300 bp on the chromosome III (Chr 3) map.

(B) Same as in (A), with Pif1 (green) and Polα (light blue) binding profiles determined in strains CY13074, CY13073, CY13284, and CY13282.

(A and B) BrdU-chip profiles were determined in strains CY12512, CY12527, CY12488, and CY12493. Statistical analysis of profile overlaps is described in Experimental Procedures. The y axis shows the signal log2 immunoprecipitation (IP)/supernatant ratios, which express enrichments in the IP fractions and are related to the magnitude of protein-DNA bindings or BrdU incorporations in the reported Chr 3 region.

(C) The profiles in the graphs express the average of the ChIP-chip binding signals for the indicated proteins in a window of 24 kb centered on each of the 141 early active DNA replication origins in the indicated genetic backgrounds (see Experimental Procedures).

(D) The magnitude of Polα, Rrm3, and Pif1 binding was determined in the experiments shown in (A) and (B) by quantitative ChIP-qPCR in the indicated genetic backgrounds on the left side of the *ARS305* (see Experimental Procedures).

See also Figure S1.

signal by 2D gel, characterized by the presence of large Ys, cruciform structures, and a cone signal (Figure 2B, yellow arrow). The cruciform structures and the cone signal have been related to aberrant replication events because of the absence of Rad53 (Lopes et al., 2001). The *sml1Δ rad53Δ pif1-m2* and *sml1Δ rad53Δ rrm3Δ* cells showed a reduction of the aberrant structures compared to *sml1Δ rad53Δ* mutants (Figures 2B and 2C). In *sml1Δ rad53Δ pif1-m2 rrm3Δ* mutants, not only the replication intermediates were less abundant due to fork movement outside the *YCL044C* locus, but the relative amount of aberrant structures was reduced compared to *sml1Δ rad53Δ* cells (Figures 2B and 2C). To confirm this observation, we analyzed early time points in *sml1Δ rad53Δ* and *sml1Δ rad53Δ pif1-m2 rrm3Δ* mutants and found that the aberrant fork structures were under-represented throughout the kinetic in the quadruple mutant *sml1Δ rad53Δ pif1-m2 rrm3Δ* (Figure S2A). Hence, Rrm3 and Pif1 are detrimental to fork movement in *rad53* mutants treated with HU. Moreover, in *rad53* mutants, the aberrant accumulation of cruciform intermediates and their derivatives migrating in the cone signal (Lopes et al., 2001) depended on Rrm3 and Pif1. Based on these conclusions, the expectation would be that ablation of *RRM3* and *PIF1* in a *rad53* background should restore replisome movement even at higher HU concentrations. We found that in cells released from G1 into 150 mM HU for 60 min, Polα immediately collapsed close to the firing point of *ARS305* in *rad53* mutants, as shown by the short ChIP-chip clusters, while in *sml1Δ rad53Δ pif1-m2 rrm3Δ* cells, Polα covered larger genomic regions as a result of replisome movement (Figure S2B).

Rrm3 and Pif1 Promote Chromosome Fragility and Cell Lethality in *rad53* Mutants Exposed to Replication Stress

In the HU-treated quadruple mutant *sml1Δ rad53Δ rrm3Δ pif1-m2*, the fork defects caused by *RAD53* ablation were

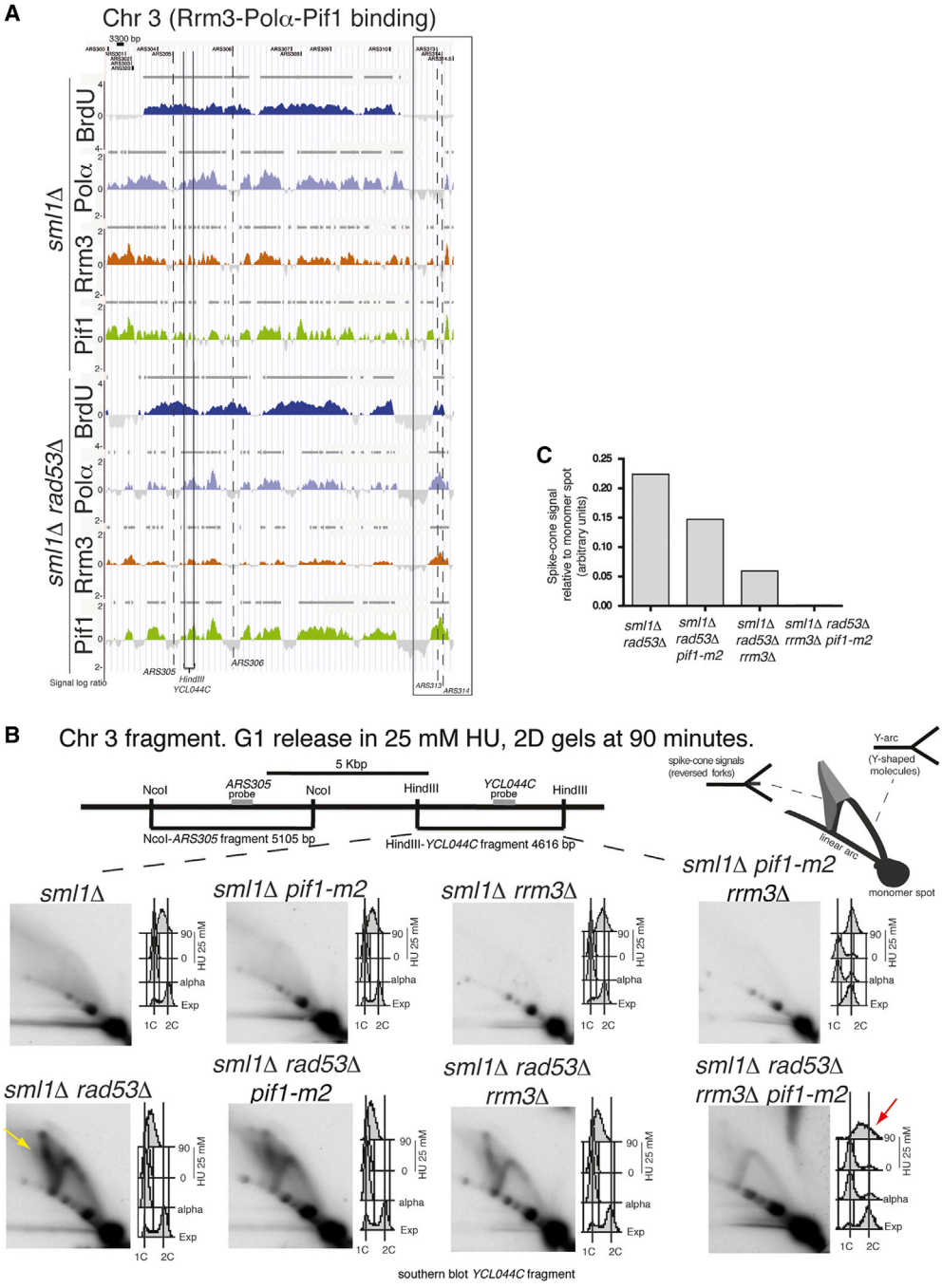

Figure 2. Fork Abnormalities in *rad53* Mutants Treated with HU Depend on Rrm3 and Pif1

(A) Polα-Flag (light blue), Rrm3-13Myc (red), and Pif1-Flag (green) binding profiles were determined in strains CY13284, CY13282, CY12470, CY12422, CY13074, and CY13073 following release from G1 into 25 mM HU for 45 min. BrdU-chip profiles were determined in strains CY12488 and CY12493. Dashed black lines and gray bars indicate origins and significant clusters, respectively, as in Figure 1A. The position of the HindIII-*YCL044C* restriction fragment is shown on the ChIP-chip maps. Chr 3, chromosome III.

(B) 2D gel analysis after in vivo psoralen crosslinking on the HindIII-*YCL044C* fragment in strains CY12445, CY13331, CY12448, CY13334, CY12443, CY13339, CY12460, and CY13342, released from G1 into 25 mM HU for 90 min. FACS profiles showing the cellular DNA content during the experiments and schematic representation of the 2D signals are shown. The yellow arrow indicates the spike or cone signal corresponding to aberrant DNA intermediates accumulating in HU in the absence of *RAD53*, while the red arrow indicates the cell-cycle progression in the quadruple mutant *sml1Δ rad53Δ rrm3Δ pif1-m2*.

(C) The intensity of the spike or cone signals detected in the 2D gels of (B) was normalized against the intensity of their monomer spots and reported into the histogram (a.u.) for the indicated strains.

See also Figure S2.

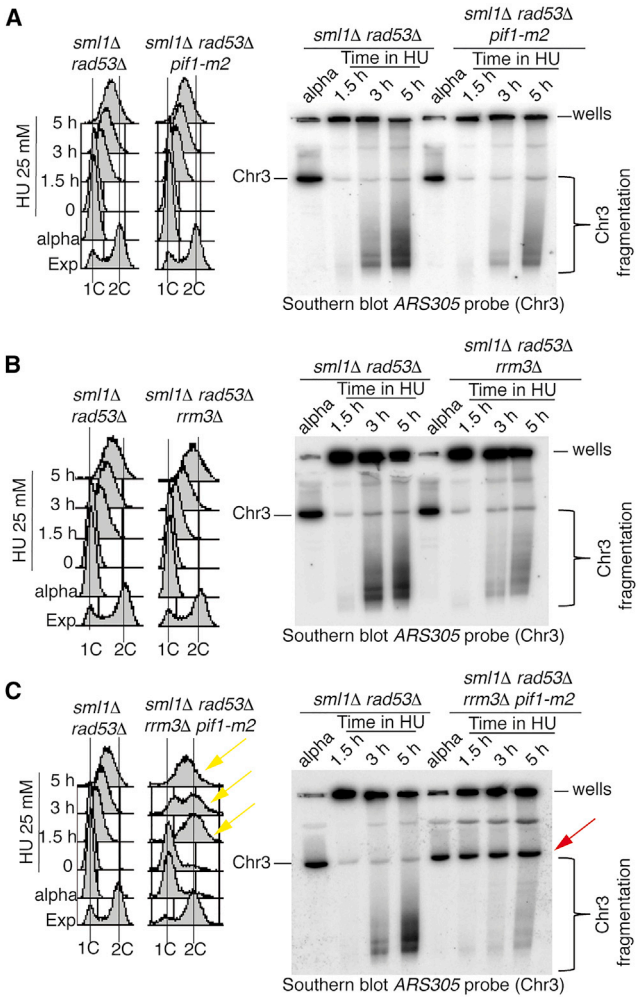

Figure 3. *RRM3* and *PIF1* Ablations Suppress Replication Stress-Induced Chromosome Fragility in *rad53* Mutants

(A–C) PFGE and Southern blotting analysis of chromosome III (Chr 3) using an *ARS305* recognizing probe in strains CY12443, CY13339, CY12460, and CY13342 at the indicated time points after a G1 release into 25 mM HU. The black line and the black bracket indicate, respectively, the migration position of the entire Chr 3 and the region of the gel in which chromosome fragmentation is detectable. The position of the wells is indicated.

(C) The red arrow in indicates Chr 3, which re-enters into the gel in the presence of HU in the *sml1Δ rad53Δ rrm3Δ pif1-m2* cells. Yellow arrows indicate cell-cycle progression into mitosis in the quadruple mutant *sml1Δ rad53Δ rrm3Δ pif1-m2*. FACS profiles are shown.

See also Figure S3.

significantly reduced; therefore, we investigated whether Rrm3, Pif1, or both contributed to the chromosome fragmentation, typical of *rad53* cells exposed to low HU doses (Hashash et al., 2011). The *sml1Δ rad53Δ*, *sml1Δ rad53Δ pif1-m2*, *sml1Δ rad53Δ rrm3Δ* and *sml1Δ rad53Δ rrm3Δ pif1-m2* strains were released from G1 into 25 mM HU and analyzed by pulsed field gel electrophoresis (PFGE) and Southern blotting at the indicated time points (Figure 3). The G1 chromosomes entered into the PFGE gel, while replicating chromosomes in HU-arrested cells were retained into the wells (Figure 3). Fluorescence-activated cell sorting (FACS) analysis showed that while *pif1-m2* and *rrm3Δ* mutations slightly influenced the bulk of DNA synthesis, in an *sml1Δ rad53Δ* background, the combination of *pif1-m2* and *rrm3Δ* mutations allowed *sml1Δ rad53Δ* cells to complete replication and progress through mitosis into the next cell cycle (Figures 3A–3C). Using PFGE, we found that in *sml1Δ rad53Δ* cells, most of chromosome III migrated in the gel in G1-arrested cells, while it was retained in the wells at 1.5 hr in HU. At 3 and 5 hr in HU, massive chromosome fragmentation appeared (Figures 3A–3C). The *pif1-m2* or *rrm3Δ* mutations partially suppressed chromosome fragmentation in *sml1Δ rad53Δ* cells (Figures 3A, 3B, and S3A). The suppression of double-stranded break (DSB) accumulation was higher when both *pif1-m2* and *rrm3Δ* mutations were introduced in the *sml1Δ rad53Δ* background and, concomitantly, chromosomes III migrated in the gel with minimal fragmentation (Figures 3C and S3A). We failed to detect chromosome III fragmentation in a *sml1Δ* WT *RAD53* background carrying the *pif1-m2*, *rrm3Δ*, or *pif1-m2 rrm3Δ* mutations (data not shown). To address whether the metaphase to anaphase transition influenced chromosome fragmentation, we performed analogous experiments in the presence of nocodazole (which blocks cells in metaphase) and obtained similar results (Figure S3B). Ablations of *PIF1* and *RRM3* suppressed chromosome fragmentation in HU-treated *rad53* cells even when *SML1* was deleted and Rrn1 was overexpressed (Figure S3C). Because *SML1* deletion and Rrn1 overexpression increase dNTP levels of at least 10-fold (Poli et al., 2012), this observation rules out that dNTP levels influence the mechanism of suppression.

We conclude that Pif1 and Rrm3 are detrimental to the integrity of replicating chromosomes in the absence of Rad53 following replication stress. These observations imply that Pif1 and Rrm3 should also be detrimental for the viability of *rad53* cells in HU. We found that the *pif1-m2* mutation alone did not influence *rad53* viability in HU (Figure 4A). Conversely, *RRM3* deletion partially rescued the HU sensitivity of *rad53* mutants, and this suppression was enhanced when both *pif1-m2* and *rrm3Δ* mutations were present (Figures 4A, S4A, and S4B). Hence, the *pif1-m2* allele exerts its suppression potential only when *RRM3* is ablated. The suppression effect of *pif1-m2* and *rrm3Δ* was specific for replication stress induced by dNTP deprivation, because they did not influence *rad53* viability following UV-induced DNA damage (Figure 4B). Moreover, the helicase-dead *rrm3-K260A* mutation suppressed the *rad53* HU sensitivity to the same extent as *RRM3* deletion, implying that the detrimental effect of Rrm3 in a *rad53* mutant background depends on Rrm3 activity (Figure 4C). It has been shown that gene gating defective mutants partially suppress the HU sensitivity of *rad53* cells (Bermejo et al., 2011). We combined *rrm3Δ* with *sac3Δ* (altered in gene gating) and found that the suppression capability of these mutations was additive in a *rad53* background, suggesting that *rrm3Δ* and *sac3Δ* influence the viability of HU-treated *rad53* cells through different mechanisms (Figure 4D). To rule out that suppression of HU sensitivity caused by the combination of *pif1-m2* and *rrm3Δ* mutations with *RAD53* deletion was due to other unknown mutations, we complemented the quadruple mutant strain *sml1Δ rad53Δ rrm3Δ pif1-m2* used in Figures 2B, 3C, 4A, 4B, and S2A with a centromeric plasmid carrying either the WT

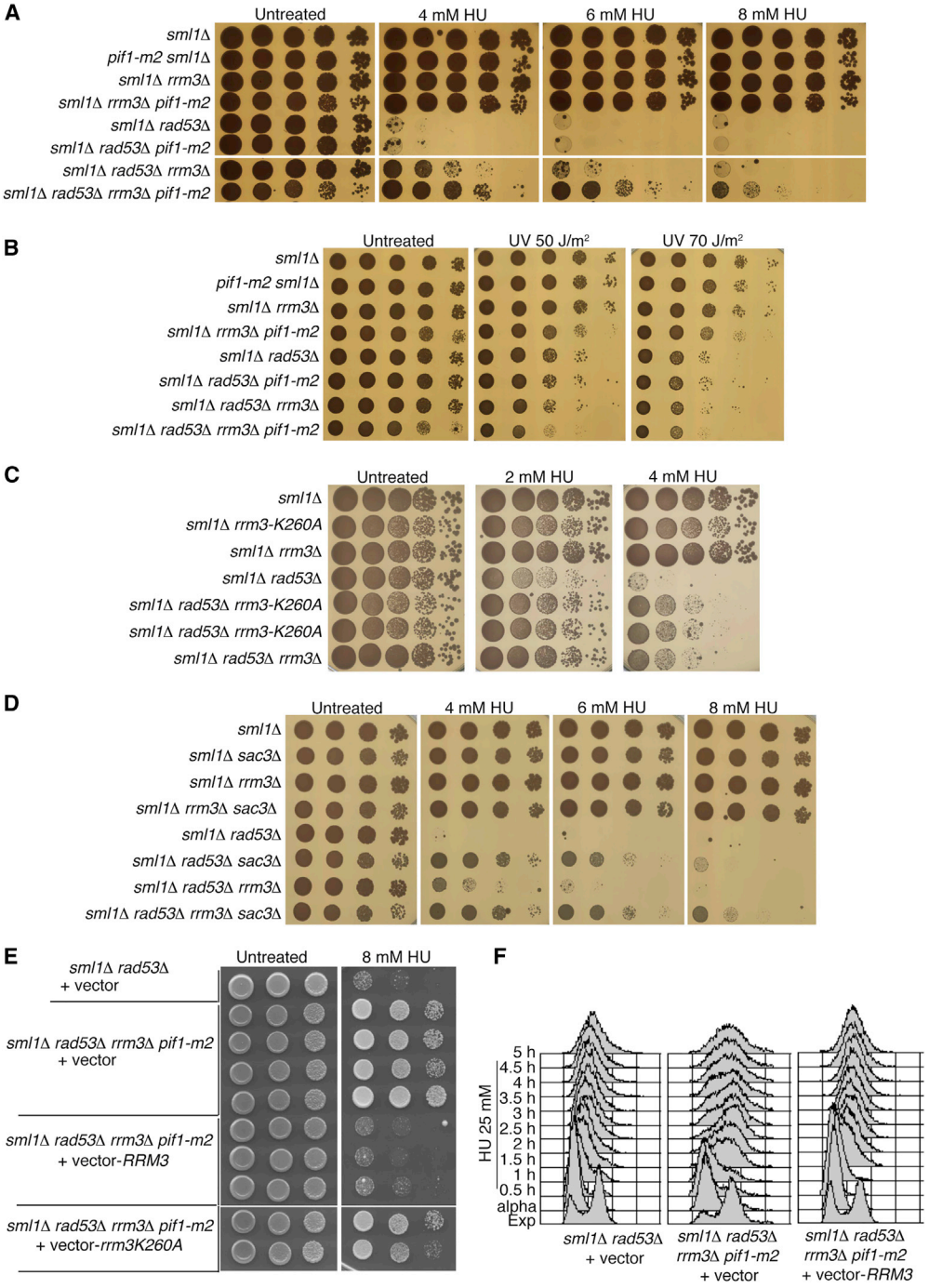

Figure 4. Rrm3 and Pif1 Are Detrimental in *rad53* Mutants under Replication Stress

(A) HU sensitivity at the indicated dosages was determined by drop assay in strains CY12445, CY13331, CY12448, CY13334, CY12443, CY13339, CY12460, and CY13342.

(B) Same as in (A) but, after cell deposition, the plates were irradiated with the indicated UV dosages (expressed in J/m^2).

(C) HU sensitivity was determined as in (A) but with strains CY12867, CY13173, CY12448, CY12865, CY13172, CY13174, and CY12460.

(D) HU sensitivity was determined as in (A) but with strains CY12445, CY12682, CY12448, CY12690, CY12674, CY12681, CY12460, and CY12689.

(E) HU sensitivity was determined as in (A) for strains CY12443 and CY13342, transformed with the indicated plasmids *YCplac111* (empty vector), *YCplac111-RRM3*, or *YCplac111-rrm3-K260A* expressing either the WT form of Rrm3 or the helicase-dead mutant allele *rrm3-K260A* (Ivessa et al., 2002).

(F) The strains CY12443 (transformed with *YCplac111*) and CY13342 (transformed with either *YCplac111* or *YCplac111-RRM3*) were arrested in G1 and released in 25 mM of HU. The cellular DNA content was determined by FACS analysis at the indicated time points.

See also Figure S4.

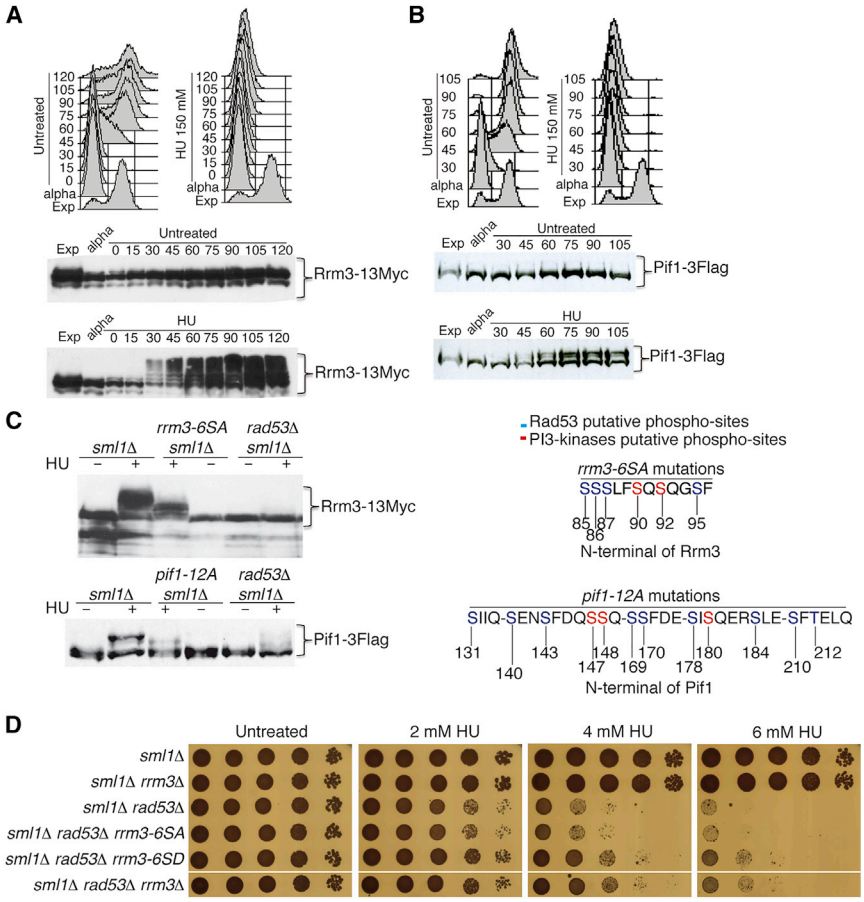

Figure 5. Rad53-Dependent Rrm3 and Pif1 Hyper-phosphorylation and Characterization of Phospho-mimicking *rrm3-6SD* and *pif1-12D* Alleles

(A) The strain CY11360 was arrested in G1 and released in the presence or absence of 150 mM HU. HU-induced hyper-phosphorylation of Rrm3-13Myc was visualized by western blotting using phospho-tag gels and anti-myc antibodies at the indicated time points. FACS profiles are shown.

(B) Same as in (A), but HU-induced hyper-phosphorylation of Pif1-6His-3Flag was analyzed in strain CY13074.

(C) The *RAD53* genetic dependence of the HU-induced Rrm3 and Pif1 hyper-phosphorylations and the phosphorylation state of the *rrm3-6SA* and *pif1-12A* mutant proteins were analyzed at 90 min from G1 release into 150 mM HU in strains CY12867, CY12953, CY12865, CY13074, CY13664, and CY13073. The Rrm3 and Pif1 protein sequences with the putative phosphorylation sites for PI3 kinases (red) or Rad53 (blue), substituted to alanine in the *rrm3-6SA* and *pif1-12A* phospho-deficient alleles or to aspartate in the corresponding phospho-mimicking alleles, are shown.

(D) HU sensitivity was determined by drop assay at the indicated HU dosages in strains CY12867, CY12448, CY12865, CY12960, CY12850, and CY12460.

See also Figures S5–S7.

RRM3 gene or the helicase-dead allele *rrm3-K260A* (Ivessa et al., 2002). We found that suppression of HU sensitivity in the *sml1Δ rad53Δ rrm3Δ pif1-m2* strain was abolished only when the WT *RRM3* gene was present (Figure 4E). When we expressed Rrm3 in the *sml1Δ rad53Δ rrm3Δ pif1-m2* strain, the replication block caused by the absence of *RAD53* and the presence of HU was restored, demonstrating that the capability of the *sml1Δ rad53Δ rrm3Δ pif1-m2* strain to replicate in 25 mM HU (Figure 3C) was due to the absence of Rrm3 (Figure 4F).

Rrm3 and Pif1 Are Phosphorylated in a Rad53-Dependent Manner following Replication Stress

Pif1 is phosphorylated in HU-treated cells (Makovets and Blackburn, 2009). We investigated whether Pif1, and eventually Rrm3, were phosphorylated under replication stress in a checkpoint-dependent manner. Rrm3-Myc and Pif1-Flag *sml1Δ* strains were released from G1 into 150 mM HU. Samples were analyzed by western blotting using phospho-tag gels to maximize the mobility shifts due to phosphorylation (Kinoshita et al., 2006). Both Rrm3 and Pif1 exhibited mobility shifts, between 30 and 45 min following the release into HU (Figures 5A and 5B). We then addressed whether the HU-induced phosphorylation events were dependent on Rad53. Rrm3-Myc and Pif1-Flag *sml1Δ* and *sml1Δ rad53Δ* strains were treated under the same conditions, and samples were taken after 90 min from the G1 release in HU (Figure 5C). We found that the mobility shifts of Rrm3 and Pif1 were abolished in the absence of Rad53. Hence, both Rrm3 and Pif1 are regulated through phosphorylation in a Rad53-dependent manner under replication stress, but these phosphorylation events are unlikely to control their bindings to forks (Figures 1A and 1B).

We then identified in the N terminus of Rrm3 six serines clustered in a sequence of 12 amino acids, which represented potential consensus motives for Rad53 and Mec1 (Figure 5C) (Smolka et al., 2007). Mutagenesis of the six serines to alanine or aspartic residues gave rise, respectively, to the phospho-defective *rrm3-6SA* or the phospho-mimicking *rrm3-6SD* alleles. In the *rrm3-6SA* mutant, the HU-induced and Rad53-dependent hyper-phosphorylated isoforms of Rrm3 were significantly reduced (Figure 5C). The protein levels of the products encoded by the *rrm3-6SA* and *rrm3-6SD* mutated genes were comparable with the ones of WT *RRM3* (Figure S5A). By comparing *rrm3-6SA* and *rrm3-6SD* mutant strains with *rrm3Δ* or WT *RRM3* cells, we found that the phospho-sites mutants did not exhibit any histone H2A or Rad53 hyper-phosphorylation when grown under unperturbed conditions (Figure S5A). Moreover, they did not show massive fork slow down at the replication fork barrier (RFB) at rDNA and at the $tRNA^A$ locus, which are typical Rrm3-dependent pausing sites (Figures S5B and S5C) (Ivessa et al., 2000, 2003). Finally, we analyzed fork pausing at the $tRNA^A$ gene in *sml1Δ*, *sml1Δ rad53Δ*, and *sml1Δ rrm3Δ* cells growing under normal conditions or following a 90 min treatment in

25 mM of HU (Figure S5D). We found that in both conditions, *sml1Δ rrm3Δ* cells were the only ones accumulating pausing signals at the *tRNA*^{A} gene locus. Hence, Rad53 and Rad53-mediated Rrm3 and Pif1 phosphorylation do not seem to influence replication across natural pausing sites. We then combined the *rrm3* phospho-site mutations with the deletion of *RAD53* and found that while the *rrm3-6SD* allele was able to rescue the HU sensitivity of *rad53* cells to the same extent as *RRM3* deletion, the *rrm3-6SA* mutation did not influence *rad53* viability in the presence of HU (Figure 5D).

We identified a region in the N terminus of Pif1 (Figure 5C, amino acids 131–212), in which 11 serine residues and 1 threonine represented putative Rad53 and Mec1 phosphorylation sites (Smolka et al., 2007). Mutagenesis of these 12 residues to alanine or aspartic acid gave rise to the *pif1-12A* and *pif1-12D* mutant alleles (Figure 5C). These mutations did not affect Pif1 protein levels, did not influence the length of the telomeres (a typical phenotype of *pif1-m2* cells [Schulz and Zakian, 1994]), and did not increase the frequency of petite cells (a read out of mitochondrial dysfunctions) (Figures S6A and S6B and data not shown). The *pif1-12A* phospho-deficient allele reduced the HU-induced and Rad53-dependent hyper-phosphorylated isoforms of Pif1 (Figure 5C). We combined the *pif1-12A* or *pif1-12D* alleles in *RRM3*, *rrm3-6SA*, and *rrm3-6SD* strains carrying two integrated copies of the galactose-inducible *rad53-D339A* dominant-negative allele (Pellicioli et al., 1999). Following *rad53-D339A* overexpression, *pif1-12A*, *rrm3-6SA*, or *pif1-12D* mutations alone did not influence cell survival in the presence of HU. Conversely, *rrm3-6SD* or the combination *rrm3-6SD pif1-12D* was able to suppress *rad53* HU sensitivity (Figure S7). The double phospho-mimicking *rrm3-6SD pif1-12D* mutant did not exhibit much better survival of HU compared to *rrm3-6SD* alone (Figure S7), likely because the phospho-mimicking mutations in *PIF1* did not fully resemble a constitutively phosphorylated gene product. Altogether, these observations suggest that Rad53 negatively regulates Rrm3 and Pif1 through phosphorylation and that this regulatory process counteracts toxic events mediated by Rrm3 and Pif1 at stalled forks.

Rrm3 and Pif1 Promote Fork Reversal in Checkpoint-Defective Cells Exposed to Replication Stress

We used psoralen crosslinking followed by electron microscopy (EM) (Neelsen et al., 2014) to visualize the fate of replication intermediates in *sml1Δ rad53Δ* and *sml1Δ rad53Δ rrm3Δ pif1-m2* mutant cells. We analyzed 165 forks in *sml1Δ rad53Δ* and found abnormal replication structures as previously described (Sogo et al., 2002). In particular, 41% were resected forks, in either hemi-replicated or gapped conformation, and contained extensive ssDNA regions (Figures 6A–6C and 6F); 10% were reversed forks (Figures 6D–6F); and 7% were broken forks (Figures 6E and 6F). We then analyzed 155 forks in *sml1Δ rad53Δ rrm3Δ pif1-m2* cells and found that 28% were resected forks, 2% were reversed forks, and 2% were broken forks (Figure 6F). We also found that while the length of the ssDNA gaps in *sml1Δ rad53Δ* cells at fork branching points was distributed around 800 nt, in *sml1Δ rad53Δ rrm3Δ pif1-m2* mutants, the gaps were significantly shorter (Figure 6G). We conclude that Rrm3 and Pif1 contribute to the accumulation of resected and reversed forks in checkpoint-defective cells.

DISCUSSION

We showed that, following replication stress, the Mec1-Rad53 axis negatively regulates the activity of Rrm3 and Pif1 helicases at stalled forks and that *RRM3* and *PIF1* ablations ameliorate checkpoint mutants, which cannot recover from HU-induced fork stalling. Our observations do not exclude that other replication factors contribute to prevent aberrant transitions at HU-induced stalled forks. Previous observations showed that both helicases assist fork progression across replication pausing elements during the unperturbed S phase. Rrm3 and Pif1 have 5′-to-3′ DNA helicase activities. Based on the polarity of the helicase activity (Bochman et al., 2010) and on its interaction with PCNA (Schmidt et al., 2002), Rrm3 may travel on the lagging strand to facilitate Okazaki fragment synthesis. However, because Rrm3 interacts also with Pol ε (Azvolinsky et al., 2006), it cannot be ruled out that at least a fraction of Rrm3 may counteract DNA synthesis on the leading strand, perhaps to promote occasional backtracking of the replisome or Pol ε-mediated proofreading (Johnson et al., 2015). *S. pombe* Pfh1 assists fork progression across pausing elements containing both non-nucleosomal DNA-protein complexes and transcribed regions (Sabouri et al., 2012), whereas *S. cerevisiae* Pif1 has been involved in resolving stable intra-molecular DNA structures such as G4 quadruplexes (Paeschke et al., 2011, 2013), facilitating Okazaki fragment processing by generating long flaps (Pike et al., 2009; Rossi et al., 2008), and preventing their intramolecular annealing (Pike et al., 2010). Accordingly, Rrm3 and Pfh1 ablations cause extensive pausing at fork barriers and transcribed regions, and Pif1 depletion affects replication across G4 quadruplex regions and Okazaki fragment processing (Fachinetti et al., 2010; Ivessa et al., 2000, 2003; Paeschke et al., 2013; Pike et al., 2009; Sabouri et al., 2012). Pif1 activity also leads to the deleterious formation of long 5′ flaps during Okazaki fragment processing in the absence of Dna2 (Budd et al., 2006; Rossi et al., 2008). Given that both Rrm3 and Pif1 have been implicated in assisting lagging strand synthesis, a logical expectation is that a Rad53-mediated inhibition of Rrm3 and Pif1 helicase activities would preferentially affect the polymerization of the lagging strand (Figure 7). This asymmetric stalled fork configuration with advanced leading strand and stable replisome- or helicase-fork complexes may facilitate, in some way, fork restart following HU removal and checkpoint deactivation. Accordingly, in WT cells, forks stalled by HU exhibited an asymmetric accumulation of approximately 100 nt of ssDNA at the fork branching point (Sogo et al., 2002).

In checkpoint mutants, Rrm3 would remain unphosphorylated and active, generating a fork configuration opposite the one of WT cell, in which the lagging strand would be more elongated than the leading one. The described scenario is consistent with the finding that when forks stall, lagging strand-bound PCNA is unloaded in a Mec1- and Rad53-dependent manner (Yu et al., 2014). A stalled fork with a protruding lagging strand might be the ideal context to trigger the formation of chicken foot-like structures at forks: if the last Okazaki fragment is processed

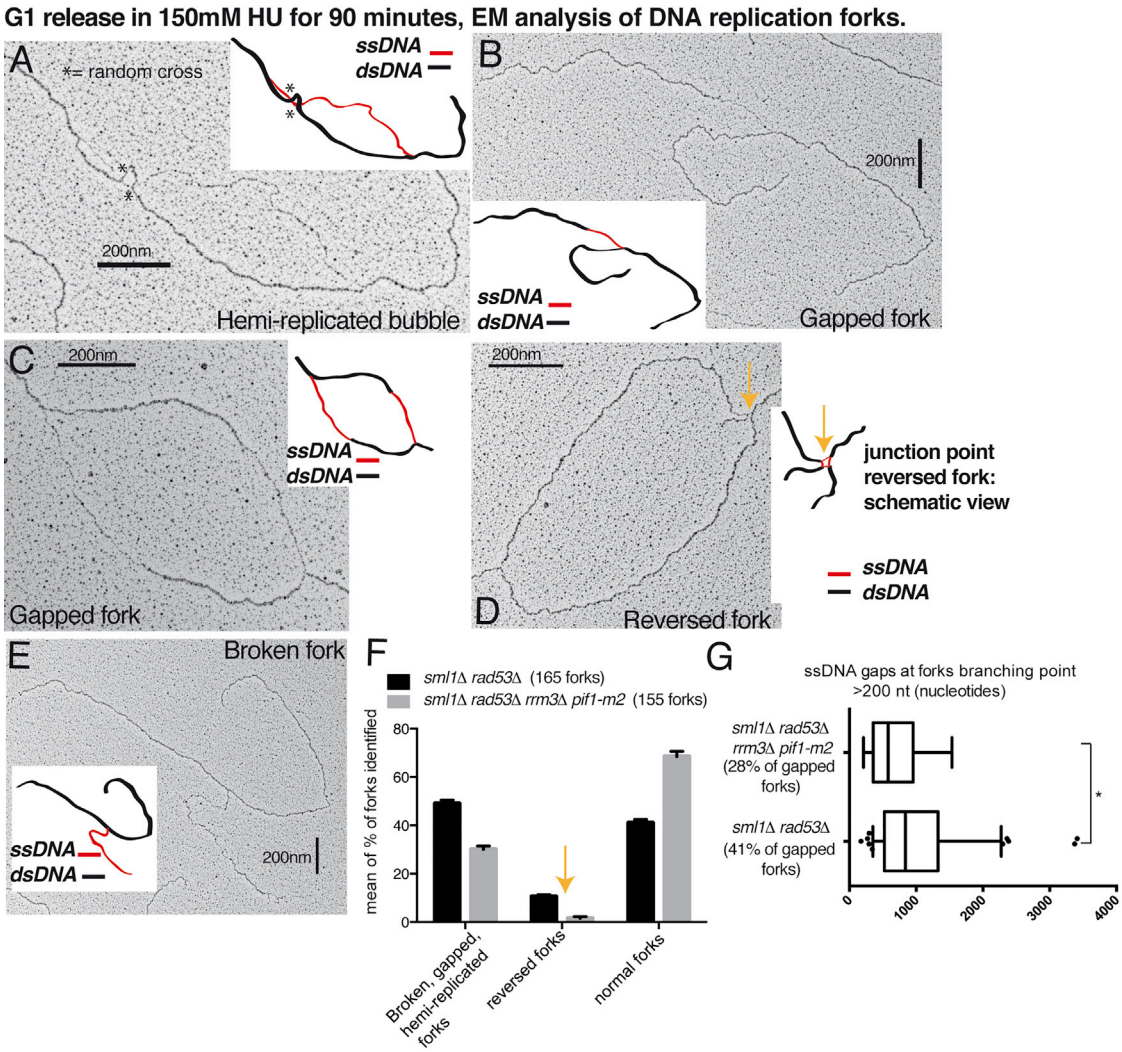

Figure 6. Rrm3 and Pif1 Contribute to Fork Abnormalities in *rad53* Cells Treated with HU

(A–E) Representative transmission electron microscopy (TEM) pictures of in vivo psoralen crosslinked DNA replication forks with different structural features (hemi-replicated forks, gapped forks, reversed forks, and broken forks), isolated from strains CY12443 and CY13342 at 90 min from G1 release into 150 mM HU. (F) A plot representing the means of the percentages and SDs of the DNA replication fork structures found in two independent experiments. At least 80 DNA replication forks were analyzed for each experiment. The number of samples (molecules) in the dataset is 165 forks for CY12443 and 155 forks for CY13342. (G) Distributions of the length of the ssDNA gaps measured at the fork branching points in the two strains. The ssDNA data representation is as follows (box plot): center line, median; box limits, 10th and 90th percentiles; whiskers, 1st and 99th percentiles; black dots, outliers. * $p < 0.05$ by two-tailed t test. Means of the percentages of gapped forks identified in the two strains in the two independent experiments are reported. The orange arrows indicate the structural features of the reversed forks and the distribution of these replication intermediates in the indicated genetic backgrounds. The 200 nm scale bars are reported in black in each TEM picture.

through the generation of a flap, then the template strands at the fork branching point would have enough space to re-anneal together, thus leading to the formation of a cruciform DNA structure in which the lagging flap is in a reversed conformation. Similar structures have been visualized in checkpoint-defective cells (Sogo et al., 2002) and may facilitate the formation of reversed forks by engaging the nascent leading strands into pairing with the lagging flaps.

The model described in Figure 7 implies that Rrm3 plays a pivotal role in fork reversal while Pif1 plays a minor role. In the absence of Pif1, it is expected that a fraction of reversed forks would still form, while it would be difficult to envisage fork reversal formation in the absence of both Rrm3 and Pif1. We found that in the absence of Rrm3, a fraction of Pif1-dependent cruciform structures still accumulate at forks in *rad53* mutants (Figure 2B). Fork reversal may still occur, although less efficiently, due to unscheduled RNA priming followed by Pif1-dependent flap elongation. Several papers analyzed the in vitro activities of Pif1 helicases on DNA replication fork-like structures (Boulé and Zakian, 2007; George et al., 2009; Ramanagoudr-Bhojappa et al., 2014). The reported results are consistent with the model proposed here.

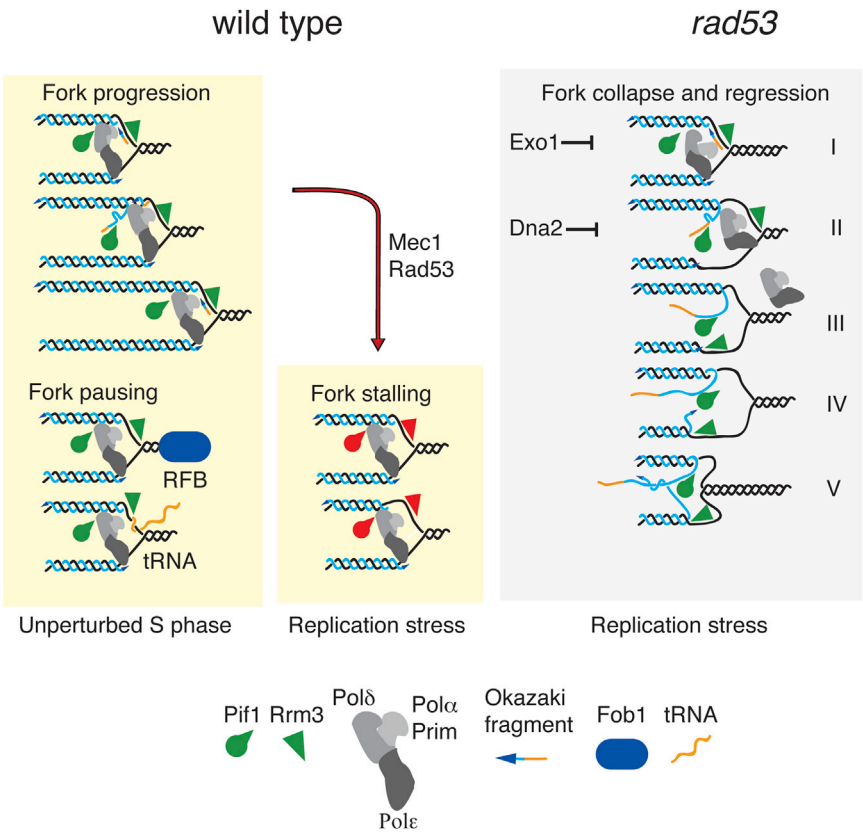

Figure 7. Model of the Rad53-Dependent Regulation of Rrm3 and Pif1 at Stalled Replication Forks

In unperturbed conditions, fork progression is assisted by Rrm3 and Pif1, particularly at pausing sites where they facilitate lagging strand synthesis. The presence of proteinaceous fork barriers like Fob1 or pausing elements like tRNAs in a head-on conformation would prevent fork pausing with an advanced lagging strand conformation. Hence, Rrm3 and Pif1 would retain their enzymatic activities to promote fork advance across the pausing sites. In the presence of HU, Rad53 inhibits Rrm3 and Pif1 on the lagging strand, leading to a stalled replication fork with an asymmetric configuration with an advanced leading strand. In HU-treated *rad53* cells, the unscheduled activities of Rrm3 and Pif1 at the stalled forks may promote fork reversal through a multistep process.

Step 1 would require the combined action of active Rrm3 and DNA primase to form an asymmetric stalled fork with the lagging strand protruding.

In step 2, the last Okazaki fragment would form a flap, thus generating a potential substrate for Pif1.

In step 3, the template strands would re-anneal at the fork branching point. The re-annealing of the template strands behind the branching point of the fork might allow Rrm3 to jump from the lagging template to the leading template and promote replisome dissociation. It is also possible that a fraction of Rrm3 is already pre-assembled at the leading template.

In step 4, while Pif1 would elongate the flaps, Rrm3 may dissociate the leading chain from the template, thus facilitating the annealing of the two nascent chains to form a reversed fork.

In step 5, reversed forks may branch migrate because of the combined action of Rrm3 and Pif1.

Exo1 and Dna2 have been shown to counteract fork reversal (Cotta-Ramusino et al., 2005; Hu et al., 2012). Both Exo1 and DNA2 have been implicated in lagging strand synthesis (Budd and Campbell, 1997; Budd et al., 1995; Tishkoff et al., 1997). According to the model described earlier, Exo1 may counteract fork reversal by resecting the lagging strand (Cotta-Ramusino et al., 2005), while Cds1 may prevent fork reversal by promoting a Dna2-dependent cleavage of regressed nascent strands (Hu et al., 2012). Our data, together with the observations in *S. pombe* (Hu et al., 2012), further suggest that fork reversal in response to replication stress represents a pathological event caused by checkpoint defects. However, in certain mammalian cell lines, fork reversal has been implicated in replication restart mechanisms under conditions causing replication stress (Berti et al., 2013; Zellweger et al., 2015).

The lagging strand replication machinery is only one of the checkpoint targets influencing stalled fork integrity. The checkpoint-mediated regulation of the gene gating apparatus represents another key event to prevent aberrant topological transitions leading to fork reversal (Bermejo et al., 2011). Moreover, in higher eukaryotes, the *ATR*-mediated regulation of *SMARCAL1* in response to replication stress has been shown to prevent *SMARCAL1*-mediated fork remodeling and *SLX4*-dependent chromosome fragmentation (Couch et al., 2013).

Our findings suggest that in WT cells, the leading protruding configuration of stalled forks would protect them from fork reversal. Rrm3 and Pif1 have been identified as key mediators of replication fork progression across the Fob1-dependent RFB at the rDNA array (Ivessa et al., 2000) and across tRNA genes (Ivessa et al., 2003). The checkpoint kinases do not seem to control fork stability at the RFB (Calzada et al., 2005) and the $tRNA^{A}$ loci, raising the possibility that the context of natural pausing is different from that of HU-induced fork stalling. Indeed, it has been shown that at the RFB, forks stall in a nearly symmetric conformation with only 3 nt protruding in the lagging strand (Gruber et al., 2000). One possibility is that Fob1, by obstructing the migration of the fork branching point, has been evolutionarily selected to avoid a fork pausing configuration dependent on the checkpoint. Hence, forks encountering the Fob1 proteinaceous blockage would pause without having to inactivate Rrm3 and Pif1 (Figure 7). Along the same lines, tRNAs transcription in a head-on conformation with the approaching forks would specifically interfere with the lagging strands, and again, forks would pause without the need to inactivate Rrm3 and Pif1 (Figure 7).

Replication fork defects and chromosome fragmentation are thought to cause cell lethality in *rad53* mutants under replication stress. *RAD53* deleted cells accumulate fork defects long before

chromosome fragmentation can be detected (Figures 2 and 3). One possibility is that in checkpoint-defective cells, the unscheduled activities of Rrm3 and Pif1 may cause a massive collapse of those forks arising from early origins. The firing of late and dormant origins, which is also typical of checkpoint mutants, might partially compensate for the aborted early replicons, but it may also lead to unscheduled clashes with transcription units in a head-on conformation. At certain genomic loci, this may cause chromosome fragility, particularly in a context in which transcription units are still tethered to the nuclear envelope (Bermejo et al., 2011). Genomic loci causing DNA replication slow down accumulate DSBs in checkpoint-defective cells (Cha and Kleckner, 2002; Hashash et al., 2011). Hence, the aberrant events at early replicons may be a pre-requisite for the subsequent chromosome fragmentation at RSZs.

EXPERIMENTAL PROCEDURES

ChIP-chip and BrdU-chip experiments were performed and protein-DNA binding profiles and BrdU profiles were generated as described (Bermejo et al., 2009a, 2009b; Katou et al., 2003). The 2D gel electrophoresis was conducted on genomic DNA after sodium azide fixation and in vivo psoralen crosslinking as described (Liberi et al., 2006). PFGE analysis was performed as described (Giannattasio et al., 2010). Supplemental Experimental Procedures are available as Supplemental Information.

ACCESSION NUMBERS

The accession number for the experimental data reported in this paper is GEO: GSE68214.

SUPPLEMENTAL INFORMATION

Supplemental Information includes Supplemental Experimental Procedures, seven figures, and one table and can be found with this article online at http://dx.doi.org/10.1016/j.celrep.2015.08.073.

AUTHOR CONTRIBUTIONS

S.E.R. and A.A. executed the experiments. W.C. analyzed the microarray data. M.F. wrote the paper and provided financial support and scientific advice. M.G. conceived and supervised the project, designed and executed the experiments, analyzed the data, and contributed to the writing of the paper.

ACKNOWLEDGMENTS

We thank V. Zakian (Princeton University) for helpful discussions and Rrm3 expressing plasmids (Ivessa et al., 2002). We thank E. Blackburn (University of California) and S. Makovets (University of Edinburgh) (Makovets and Blackburn, 2009) for Pif1 plasmids. We also thank G. Liberi (CNR), D. Branzei (IFOM), and J. Niska (IFOM), for helpful discussions and S. Minardi (IFOM) for technological support. A.A. is supported by an AIRC fellowship. The work was supported by grants from AIRC, Telethon-Italy, and the European Commission to M.F.

Received: April 24, 2015
Revised: August 7, 2015
Accepted: August 26, 2015
Published: September 24, 2015

REFERENCES

Azvolinsky, A., Dunaway, S., Torres, J.Z., Bessler, J.B., and Zakian, V.A. (2006). The *S. cerevisiae* Rrm3p DNA helicase moves with the replication fork and affects replication of all yeast chromosomes. Genes Dev. *20*, 3104–3116.

Azvolinsky, A., Giresi, P.G., Lieb, J.D., and Zakian, V.A. (2009). Highly transcribed RNA polymerase II genes are impediments to replication fork progression in *Saccharomyces cerevisiae*. Mol. Cell *34*, 722–734.

Bermejo, R., Capra, T., Gonzalez-Huici, V., Fachinetti, D., Cocito, A., Natoli, G., Katou, Y., Mori, H., Kurokawa, K., Shirahige, K., and Foiani, M. (2009a). Genome-organizing factors Top2 and Hmo1 prevent chromosome fragility at sites of S phase transcription. Cell *138*, 870–884.

Bermejo, R., Katou, Y.M., Shirahige, K., and Foiani, M. (2009b). ChIP-on-chip analysis of DNA topoisomerases. Methods Mol. Biol. *582*, 103–118.

Bermejo, R., Capra, T., Jossen, R., Colosio, A., Frattini, C., Carotenuto, W., Cocito, A., Doksani, Y., Klein, H., Gómez-González, B., et al. (2011). The replication checkpoint protects fork stability by releasing transcribed genes from nuclear pores. Cell *146*, 233–246.

Berti, M., Ray Chaudhuri, A., Thangavel, S., Gomathinayagam, S., Kenig, S., Vujanovic, M., Odreman, F., Glatter, T., Graziano, S., Mendoza-Maldonado, R., et al. (2013). Human RECQ1 promotes restart of replication forks reversed by DNA topoisomerase I inhibition. Nat. Struct. Mol. Biol. *20*, 347–354.

Bochman, M.L., Sabouri, N., and Zakian, V.A. (2010). Unwinding the functions of the Pif1 family helicases. DNA Repair (Amst.) *9*, 237–249.

Boulé, J.B., and Zakian, V.A. (2007). The yeast Pif1p DNA helicase preferentially unwinds RNA DNA substrates. Nucleic Acids Res. *35*, 5809–5818.

Branzei, D., and Foiani, M. (2009). The checkpoint response to replication stress. DNA Repair (Amst.) *8*, 1038–1046.

Budd, M.E., and Campbell, J.L. (1997). A yeast replicative helicase, Dna2 helicase, interacts with yeast FEN-1 nuclease in carrying out its essential function. Mol. Cell. Biol. *17*, 2136–2142.

Budd, M.E., Choe, W.C., and Campbell, J.L. (1995). DNA2 encodes a DNA helicase essential for replication of eukaryotic chromosomes. J. Biol. Chem. *270*, 26766–26769.

Budd, M.E., Reis, C.C., Smith, S., Myung, K., and Campbell, J.L. (2006). Evidence suggesting that Pif1 helicase functions in DNA replication with the Dna2 helicase/nuclease and DNA polymerase delta. Mol. Cell. Biol. *26*, 2490–2500.

Calzada, A., Hodgson, B., Kanemaki, M., Bueno, A., and Labib, K. (2005). Molecular anatomy and regulation of a stable replisome at a paused eukaryotic DNA replication fork. Genes Dev. *19*, 1905–1919.

Casper, A.M., Nghiem, P., Arlt, M.F., and Glover, T.W. (2002). ATR regulates fragile site stability. Cell *111*, 779–789.

Cha, R.S., and Kleckner, N. (2002). ATR homolog Mec1 promotes fork progression, thus averting breaks in replication slow zones. Science *297*, 602–606.

Cobb, J.A., Schleker, T., Rojas, V., Bjergbaek, L., Tercero, J.A., and Gasser, S.M. (2005). Replisome instability, fork collapse, and gross chromosomal rearrangements arise synergistically from Mec1 kinase and RecQ helicase mutations. Genes Dev. *19*, 3055–3069.

Cotta-Ramusino, C., Fachinetti, D., Lucca, C., Doksani, Y., Lopes, M., Sogo, J., and Foiani, M. (2005). Exo1 processes stalled replication forks and counteracts fork reversal in checkpoint-defective cells. Mol. Cell *17*, 153–159.

Couch, F.B., Bansbach, C.E., Driscoll, R., Luzwick, J.W., Glick, G.G., Bétous, R., Carroll, C.M., Jung, S.Y., Qin, J., Cimprich, K.A., and Cortez, D. (2013). ATR phosphorylates SMARCAL1 to prevent replication fork collapse. Genes Dev. *27*, 1610–1623.

De Piccoli, G., Katou, Y., Itoh, T., Nakato, R., Shirahige, K., and Labib, K. (2012). Replisome stability at defective DNA replication forks is independent of S phase checkpoint kinases. Mol. Cell *45*, 696–704.

Deshpande, A.M., and Newlon, C.S. (1996). DNA replication fork pause sites dependent on transcription. Science *272*, 1030–1033.

Dewar, J.M., and Lydall, D. (2010). Pif1- and Exo1-dependent nucleases coordinate checkpoint activation following telomere uncapping. EMBO J. *29*, 4020–4034.

Doe, C.L., Ahn, J.S., Dixon, J., and Whitby, M.C. (2002). Mus81-Eme1 and Rqh1 involvement in processing stalled and collapsed replication forks. J. Biol. Chem. *277*, 32753–32759.

Fachinetti, D., Bermejo, R., Cocito, A., Minardi, S., Katou, Y., Kanoh, Y., Shirahige, K., Azvolinsky, A., Zakian, V.A., and Foiani, M. (2010). Replication termination at eukaryotic chromosomes is mediated by Top2 and occurs at genomic loci containing pausing elements. Mol. Cell *39*, 595–605.

Feng, W., Collingwood, D., Boeck, M.E., Fox, L.A., Alvino, G.M., Fangman, W.L., Raghuraman, M.K., and Brewer, B.J. (2006). Genomic mapping of single-stranded DNA in hydroxyurea-challenged yeasts identifies origins of replication. Nat. Cell Biol. *8*, 148–155.

Forment, J.V., Blasius, M., Guerini, I., and Jackson, S.P. (2011). Structure-specific DNA endonuclease Mus81/Eme1 generates DNA damage caused by Chk1 inactivation. PLoS ONE *6*, e23517.

Froget, B., Blaisonneau, J., Lambert, S., and Baldacci, G. (2008). Cleavage of stalled forks by fission yeast Mus81/Eme1 in absence of DNA replication checkpoint. Mol. Biol. Cell *19*, 445–456.

George, T., Wen, Q., Griffiths, R., Ganesh, A., Meuth, M., and Sanders, C.M. (2009). Human Pif1 helicase unwinds synthetic DNA structures resembling stalled DNA replication forks. Nucleic Acids Res. *37*, 6491–6502.

Giannattasio, M., Follonier, C., Tourrière, H., Puddu, F., Lazzaro, F., Pasero, P., Lopes, M., Plevani, P., and Muzi-Falconi, M. (2010). Exo1 competes with repair synthesis, converts NER intermediates to long ssDNA gaps, and promotes checkpoint activation. Mol. Cell *40*, 50–62.

Gruber, M., Wellinger, R.E., and Sogo, J.M. (2000). Architecture of the replication fork stalled at the 3′ end of yeast ribosomal genes. Mol. Cell. Biol. *20*, 5777–5787.

Hashash, N., Johnson, A.L., and Cha, R.S. (2011). Regulation of fragile sites expression in budding yeast by MEC1, RRM3 and hydroxyurea. J. Cell Sci. *124*, 181–185.

Hu, J., Sun, L., Shen, F., Chen, Y., Hua, Y., Liu, Y., Zhang, M., Hu, Y., Wang, Q., Xu, W., et al. (2012). The intra-S phase checkpoint targets Dna2 to prevent stalled replication forks from reversing. Cell *149*, 1221–1232.

Huang, M., Zhou, Z., and Elledge, S.J. (1998). The DNA replication and damage checkpoint pathways induce transcription by inhibition of the Crt1 repressor. Cell *94*, 595–605.

Ivessa, A.S., Zhou, J.Q., and Zakian, V.A. (2000). The *Saccharomyces* Pif1p DNA helicase and the highly related Rrm3p have opposite effects on replication fork progression in ribosomal DNA. Cell *100*, 479–489.

Ivessa, A.S., Zhou, J.Q., Schulz, V.P., Monson, E.K., and Zakian, V.A. (2002). *Saccharomyces* Rrm3p, a 5′ to 3′ DNA helicase that promotes replication fork progression through telomeric and subtelomeric DNA. Genes Dev. *16*, 1383–1396.

Ivessa, A.S., Lenzmeier, B.A., Bessler, J.B., Goudsouzian, L.K., Schnakenberg, S.L., and Zakian, V.A. (2003). The *Saccharomyces cerevisiae* helicase Rrm3p facilitates replication past nonhistone protein-DNA complexes. Mol. Cell *12*, 1525–1536.

Johnson, R.E., Klassen, R., Prakash, L., and Prakash, S. (2015). A major role of DNA polymerase δ in replication of both the leading and lagging DNA strands. Mol. Cell *59*, 163–175.

Katou, Y., Kanoh, Y., Bando, M., Noguchi, H., Tanaka, H., Ashikari, T., Sugimoto, K., and Shirahige, K. (2003). S-phase checkpoint proteins Tof1 and Mrc1 form a stable replication-pausing complex. Nature *424*, 1078–1083.

Kinoshita, E., Kinoshita-Kikuta, E., Takiyama, K., and Koike, T. (2006). Phosphate-binding tag, a new tool to visualize phosphorylated proteins. Mol. Cell. Proteomics *5*, 749–757.

Krakoff, I.H., Brown, N.C., and Reichard, P. (1968). Inhibition of ribonucleoside diphosphate reductase by hydroxyurea. Cancer Res. *28*, 1559–1565.

Liberi, G., Cotta-Ramusino, C., Lopes, M., Sogo, J., Conti, C., Bensimon, A., and Foiani, M. (2006). Methods to study replication fork collapse in budding yeast. Methods Enzymol. *409*, 442–462.

Lopes, M., Cotta-Ramusino, C., Pellicioli, A., Liberi, G., Plevani, P., Muzi-Falconi, M., Newlon, C.S., and Foiani, M. (2001). The DNA replication checkpoint response stabilizes stalled replication forks. Nature *412*, 557–561.

Lopes, M., Foiani, M., and Sogo, J.M. (2006). Multiple mechanisms control chromosome integrity after replication fork uncoupling and restart at irreparable UV lesions. Mol. Cell *21*, 15–27.

Lucca, C., Vanoli, F., Cotta-Ramusino, C., Pellicioli, A., Liberi, G., Haber, J., and Foiani, M. (2004). Checkpoint-mediated control of replisome-fork association and signalling in response to replication pausing. Oncogene *23*, 1206–1213.

Makovets, S., and Blackburn, E.H. (2009). DNA damage signalling prevents deleterious telomere addition at DNA breaks. Nat. Cell Biol. *11*, 1383–1386.

Matsuda, K., Makise, M., Sueyasu, Y., Takehara, M., Asano, T., and Mizushima, T. (2007). Yeast two-hybrid analysis of the origin recognition complex of *Saccharomyces cerevisiae*: interaction between subunits and identification of binding proteins. FEMS Yeast Res. *7*, 1263–1269.

Neelsen, K.J., Chaudhuri, A.R., Follonier, C., Herrador, R., and Lopes, M. (2014). Visualization and interpretation of eukaryotic DNA replication intermediates in vivo by electron microscopy. Methods Mol. Biol. *1094*, 177–208.

Paeschke, K., Capra, J.A., and Zakian, V.A. (2011). DNA replication through G-quadruplex motifs is promoted by the *Saccharomyces cerevisiae* Pif1 DNA helicase. Cell *145*, 678–691.

Paeschke, K., Bochman, M.L., Garcia, P.D., Cejka, P., Friedman, K.L., Kowalczykowski, S.C., and Zakian, V.A. (2013). Pif1 family helicases suppress genome instability at G-quadruplex motifs. Nature *497*, 458–462.

Pellicioli, A., Lucca, C., Liberi, G., Marini, F., Lopes, M., Plevani, P., Romano, A., Di Fiore, P.P., and Foiani, M. (1999). Activation of Rad53 kinase in response to DNA damage and its effect in modulating phosphorylation of the lagging strand DNA polymerase. EMBO J. *18*, 6561–6572.

Pike, J.E., Burgers, P.M., Campbell, J.L., and Bambara, R.A. (2009). Pif1 helicase lengthens some Okazaki fragment flaps necessitating Dna2 nuclease/helicase action in the two-nuclease processing pathway. J. Biol. Chem. *284*, 25170–25180.

Pike, J.E., Henry, R.A., Burgers, P.M., Campbell, J.L., and Bambara, R.A. (2010). An alternative pathway for Okazaki fragment processing: resolution of fold-back flaps by Pif1 helicase. J. Biol. Chem. *285*, 41712–41723.

Poli, J., Tsaponina, O., Crabbé, L., Keszthelyi, A., Pantesco, V., Chabes, A., Lengronne, A., and Pasero, P. (2012). dNTP pools determine fork progression and origin usage under replication stress. EMBO J. *31*, 883–894.

Ramanagoudr-Bhojappa, R., Byrd, A.K., Dahl, C., and Raney, K.D. (2014). Yeast Pif1 accelerates annealing of complementary DNA strands. Biochemistry *53*, 7659–7669.

Rossi, M.L., Pike, J.E., Wang, W., Burgers, P.M., Campbell, J.L., and Bambara, R.A. (2008). Pif1 helicase directs eukaryotic Okazaki fragments toward the two-nuclease cleavage pathway for primer removal. J. Biol. Chem. *283*, 27483–27493.

Sabouri, N., McDonald, K.R., Webb, C.J., Cristea, I.M., and Zakian, V.A. (2012). DNA replication through hard-to-replicate sites, including both highly transcribed RNA Pol II and Pol III genes, requires the *S. pombe* Pfh1 helicase. Genes Dev. *26*, 581–593.

Santocanale, C., and Diffley, J.F. (1998). A Mec1- and Rad53-dependent checkpoint controls late-firing origins of DNA replication. Nature *395*, 615–618.

Schmidt, K.H., Derry, K.L., and Kolodner, R.D. (2002). *Saccharomyces cerevisiae* RRM3, a 5′ to 3′ DNA helicase, physically interacts with proliferating cell nuclear antigen. J. Biol. Chem. *277*, 45331–45337.

Schulz, V.P., and Zakian, V.A. (1994). The *Saccharomyces* PIF1 DNA helicase inhibits telomere elongation and de novo telomere formation. Cell *76*, 145–155.

Shirahige, K., Hori, Y., Shiraishi, K., Yamashita, M., Takahashi, K., Obuse, C., Tsurimoto, T., and Yoshikawa, H. (1998). Regulation of DNA-replication origins during cell-cycle progression. Nature *395*, 618–621.

Smolka, M.B., Albuquerque, C.P., Chen, S.H., and Zhou, H. (2007). Proteome-wide identification of in vivo targets of DNA damage checkpoint kinases. Proc. Natl. Acad. Sci. USA *104*, 10364–10369.

Sogo, J.M., Lopes, M., and Foiani, M. (2002). Fork reversal and ssDNA accumulation at stalled replication forks owing to checkpoint defects. Science *297*, 599–602.

Sun, Z., Fay, D.S., Marini, F., Foiani, M., and Stern, D.F. (1996). Spk1/Rad53 is regulated by Mec1-dependent protein phosphorylation in DNA replication and damage checkpoint pathways. Genes Dev. *10*, 395–406.

Syljuåsen, R.G., Sørensen, C.S., Hansen, L.T., Fugger, K., Lundin, C., Johansson, F., Helleday, T., Sehested, M., Lukas, J., and Bartek, J. (2005). Inhibition of human Chk1 causes increased initiation of DNA replication, phosphorylation of ATR targets, and DNA breakage. Mol. Cell. Biol. *25*, 3553–3562.

Tishkoff, D.X., Boerger, A.L., Bertrand, P., Filosi, N., Gaida, G.M., Kane, M.F., and Kolodner, R.D. (1997). Identification and characterization of *Saccharomyces cerevisiae* EXO1, a gene encoding an exonuclease that interacts with MSH2. Proc. Natl. Acad. Sci. USA *94*, 7487–7492.

Toledo, L.I., Altmeyer, M., Rask, M.B., Lukas, C., Larsen, D.H., Povlsen, L.K., Bekker-Jensen, S., Mailand, N., Bartek, J., and Lukas, J. (2013). ATR prohibits replication catastrophe by preventing global exhaustion of RPA. Cell *155*, 1088–1103.

Yu, C., Gan, H., Han, J., Zhou, Z.X., Jia, S., Chabes, A., Farrugia, G., Ordog, T., and Zhang, Z. (2014). Strand-specific analysis shows protein binding at replication forks and PCNA unloading from lagging strands when forks stall. Mol. Cell *56*, 551–563.

Zegerman, P., and Diffley, J.F. (2010). Checkpoint-dependent inhibition of DNA replication initiation by Sld3 and Dbf4 phosphorylation. Nature *467*, 474–478.

Zellweger, R., Dalcher, D., Mutreja, K., Berti, M., Schmid, J.A., Herrador, R., Vindigni, A., and Lopes, M. (2015). Rad51-mediated replication fork reversal is a global response to genotoxic treatments in human cells. J. Cell Biol. *208*, 563–579.

Zhao, X., and Rothstein, R. (2002). The Dun1 checkpoint kinase phosphorylates and regulates the ribonucleotide reductase inhibitor Sml1. Proc. Natl. Acad. Sci. USA *99*, 3746–3751.

Cell Reports

Supplemental Information

Rad53-Mediated Regulation of Rrm3 and Pif1 DNA Helicases Contributes to Prevention of Aberrant Fork Transitions under Replication Stress

Silvia Emma Rossi, Arta Ajazi, Walter Carotenuto, Marco Foiani, and Michele Giannattasio

Supplemental information

Supplemental data

Rossi et al. Supplemental Figure S1

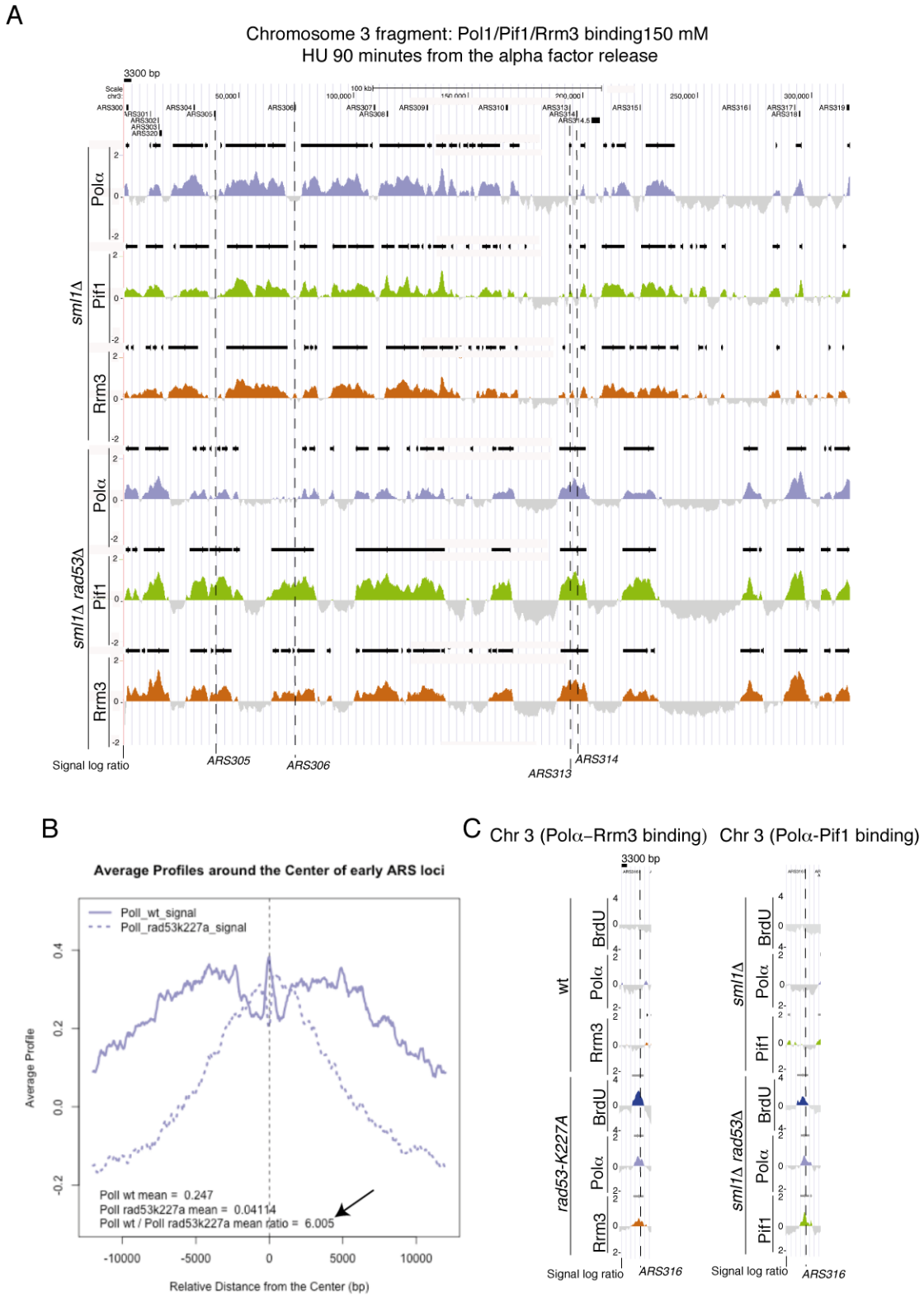

Figure S1. Rrm3 and Pif1 are replisome components under replication stress and are recruited at the late origin *ARS316*, which is fired in HU in the absence of Rad53 (related to Figure 1). A) Rrm3 and Pif1 are replisome components under replication stress. Polα-Flag (light blue), Pif1-Flag (green) and Rrm3-13Myc (red) binding profiles were determined by ChIP on chip in CY13284, CY13282, CY13074, CY13073, CY12470 and CY12422 strains, released from G1 into 150 mM of HU for 90 minutes. The y-axis show the enrichment signals expressed as ratio log2 IP/SUP of *loci* significantly enriched in the IP fractions. The horizontal black bars indicate statistically significative binding clusters. X-axis represents chromosomal coordinates. Early (*ARS305* and *ARS306*) and dormant origins (*ARS313* and *ARS314*) are marked by dashed black lines. The space between two light blue lines in the chromosome map corresponds to 3,3 kbp. **B) DNA polymerase alpha binding to flanking regions of 141 active *ARSs* is reduced in *rad53* mutants treated with high HU doses**. The area below the profiles showed in the first plot in the main figure 1C of the manuscript has been measured. The area values measured are directly linked to the magnitude of DNA polymerase alpha binding to 141 *ARSs* in the indicated genetic background. A black arrow indicates the ratio of DNA Polymerase alpha binding in wild type vs *rad53-K227A* cells in the indicated experimental condition. As it may be noticed DNA polymerase alpha binds 6 times less in *rad53-K227A* compared to wild type cells to 141 active *ARSs*. **C)** Binding profiles (enrichment signal log2 IP/SUP ratio) of Polα (light blue), Pif1 (light green), Rrm3 (red), determined by ChIP on chip and BrdU incorporation profiles (dark blue) determined by ssDNA-BrdU IP on chip (enrichment signal log2 IP/SUP ratio), in the same experiments of Figure 1A-B are

shown.

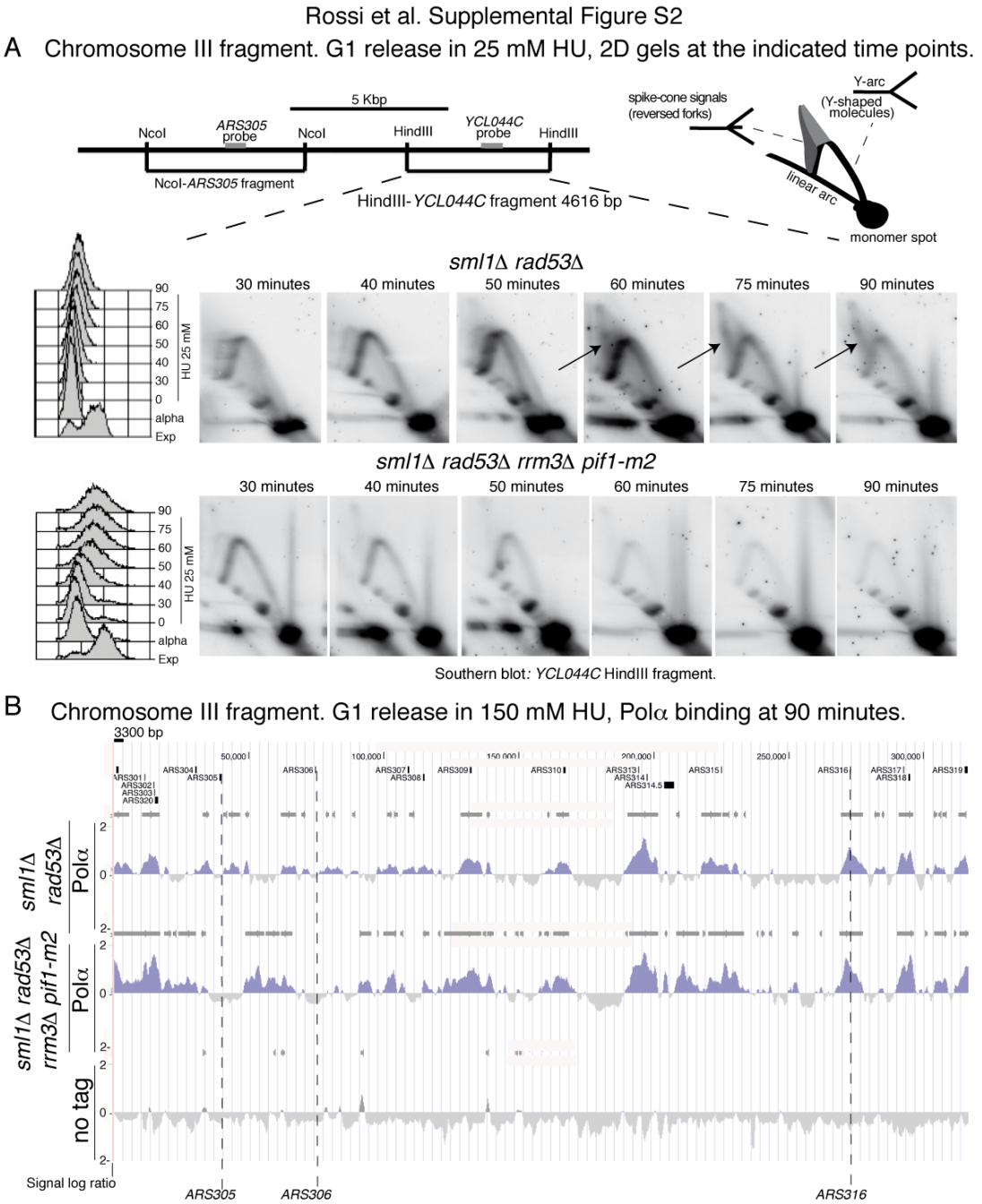

Figure S2. Rrm3 and Pif1 promote fork stalling and fork reversal in *rad53* mutants under replication stress, (related to Figure 2).

A) The strains *sml1Δ rad53Δ* (CY12443) and *sml1Δ rad53Δ rrm3Δ pif1-m2* (CY13342) have been synchronized in G1 and released into the cell cycle in the presence of 25 mM of HU. DNA replication intermediates (accumulating on the HindIII-*YCL044C* fragment schematically represented in the figure), have been analyzed by neutral-neutral 2D gels on *in-vivo* psoralen cross-linked genomic DNA at the indicated time points. FACS profiles showing the cellular DNA contents during

the experiment are reported. A schematic representation of the 2D gel signals detected in these experimental conditions is shown. Black arrows indicate the accumulation of the spike/cone signal, which represents the reversed forks, which accumulate in *rad53* cells under replication stress. **B)** The strains *sml1Δ rad53Δ* (CY13282), *sml1Δ rad53Δ rrm3Δ pif1-m2* (CY13650) carrying the *POL1-6His-3Flag* allele have been released from G1 into 150 mM HU for 60 minutes. Polα binding profiles (light blue), determined by ChIP on chip and relative to the indicated region of the chromosome III are shown. Y-axis shows the signal log2 IP/SUP ratio, which expresses the magnitude of protein-DNA binding in the chromosome *loci* represented (see experimental procedures). Dashed black lines indicate the positions of the early origins *AR305* and *ARS306* and the late origin *ARS316,* which is fired (and bound by Polα) in HU only in checkpoint defective cells.

Rossi et al Supplemental Figure S3

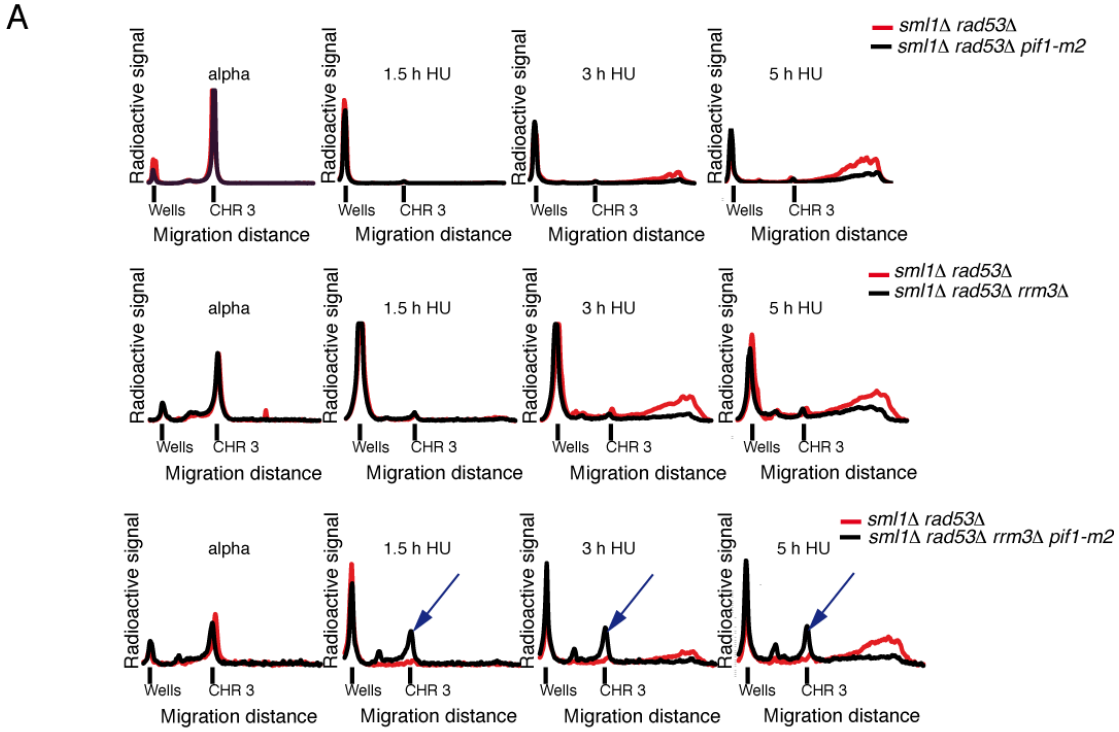

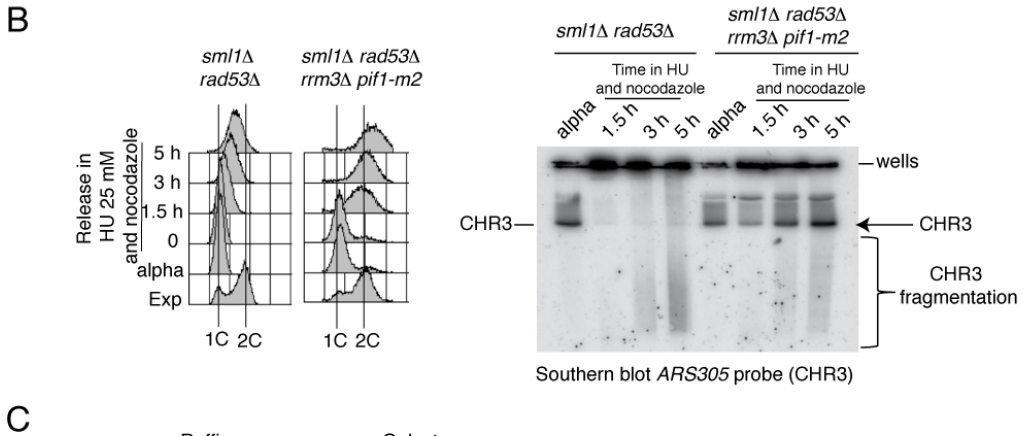

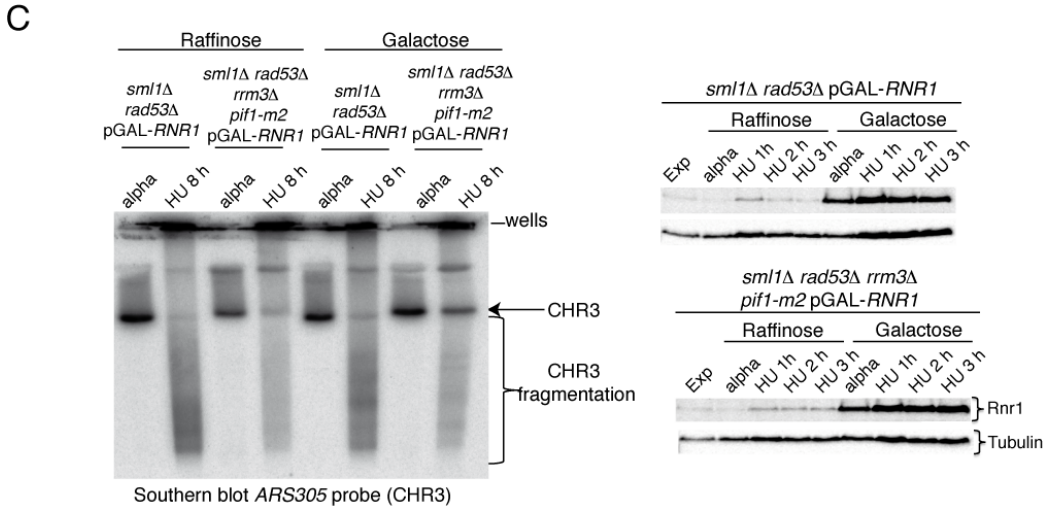

Figure S3. *RRM3* and *PIF1* ablations suppress chromosome fragmentation in *rad53* mutants exposed to replication stress, (related to Figure 3).

A) Quantitative profiles of the PFGE experiments shown in Figure 3 are reported. The intensity of the radioactive signal in each line of the PFGE gels shown in Figure 3 is plotted against the migration distance. In order to quantify and better appreciate the difference in the chromosome fragmentation between different strains, quantitative profiles of the indicated strains analyzed at different time points are overlapped. Blue arrows indicate the signals corresponding to the chromosome III, which re-enters into the gel in the quadruple mutant *sml1Δ rad53Δ rrm3Δ pif1-m2* (CY13342) treated with HU. **B) The ablation of the Pif1 helicases suppresses the chromosome fragmentation observed in *rad53* mutants treated with 25 mM of HU in the first cell cycle.** CY12443 and CY13342 strains were synchronized in G1 and released into S-phase in the presence of 25 mM of HU and nocodazole (20 µg/ml). The migration pattern of chromosome III was analyzed, at the indicated time points, by PFGE and southern blotting, using an *ARS305* recognizing probe. A black arrow indicates the southern blot signal of the chromosome III, which re-enters in the gel in HU only in the strain CY13342. The region of the gel in which chromosome fragmentation is visible is indicated by a black bracket. Position of the wells is shown. FACS profiles with the cellular DNA content during the experiment are shown. **C) High dNTPs levels do not alter the chromosome fragility induced in *rad53* mutants treated with low HU doses.** CY14076 and CY14077 strains, overexpressing the *RNR1* gene under the control of the *GAL1/GAL10* promoter, were released from a G1 arrest into 25 mM of HU for 8 hours, in the presence or absence of galactose. Chromosome III migration pattern has been analyzed by PFGE and southern blotting using an *ARS305* recognizing probe, at the indicated time points. A black arrow indicates the southern blot signal corresponding to the chromosome III, which re-enters in the gel in HU only in the strain CY14077. The region of the gel in which chromosome fragmentation is visible is indicated by a black bracket. Position of the wells is shown. In the lower panel Rnr1 protein levels have been monitored by western blotting, using anti-Rnr1 antibodies and tubulin was used as loading control.

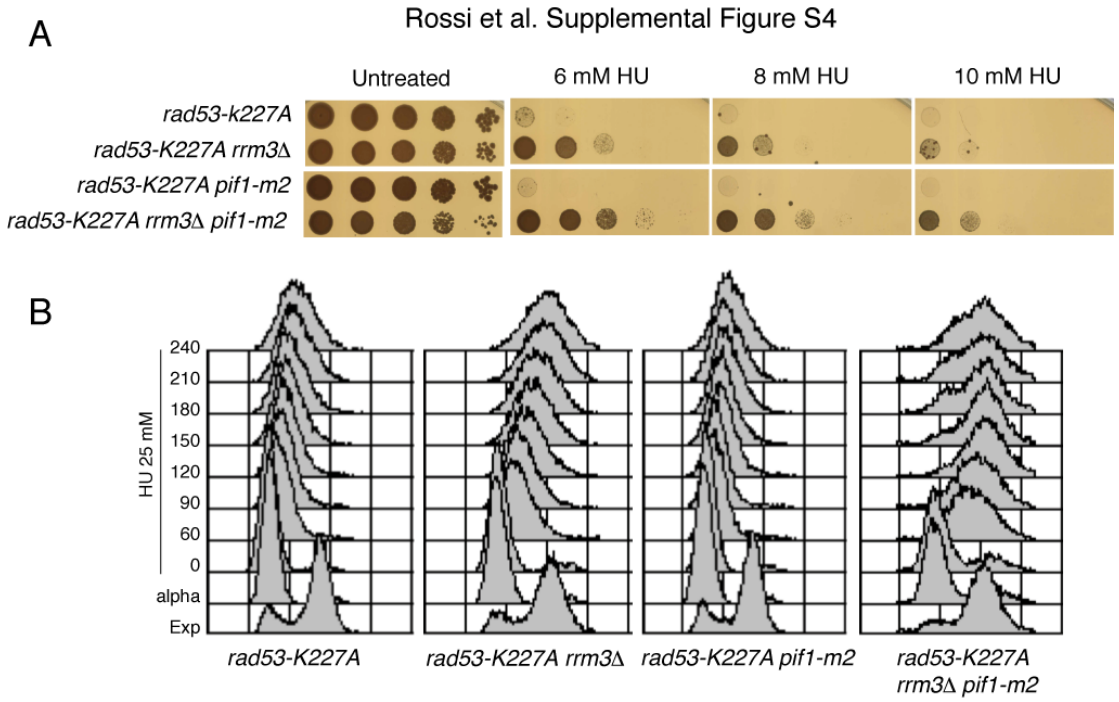

Figure S4. Ablation of the Pif1 helicases suppresses the HU sensitivity and DNA replication forks arrest induced by treatment of *rad53-K227A* mutant cells with low HU doses (related to Figure 4).

A) HU sensitivity of CY12404, CY12406, CY13735 and CY13738 strains has been determined by drop-assay, at the indicated HU dosages. **B)** The same strains as in A have been synchronized in G1 and released into S-phase in the presence of 25 mM of HU. Samples were collected at the indicated time points, and the cellular DNA content has been determined by FACS analysis.

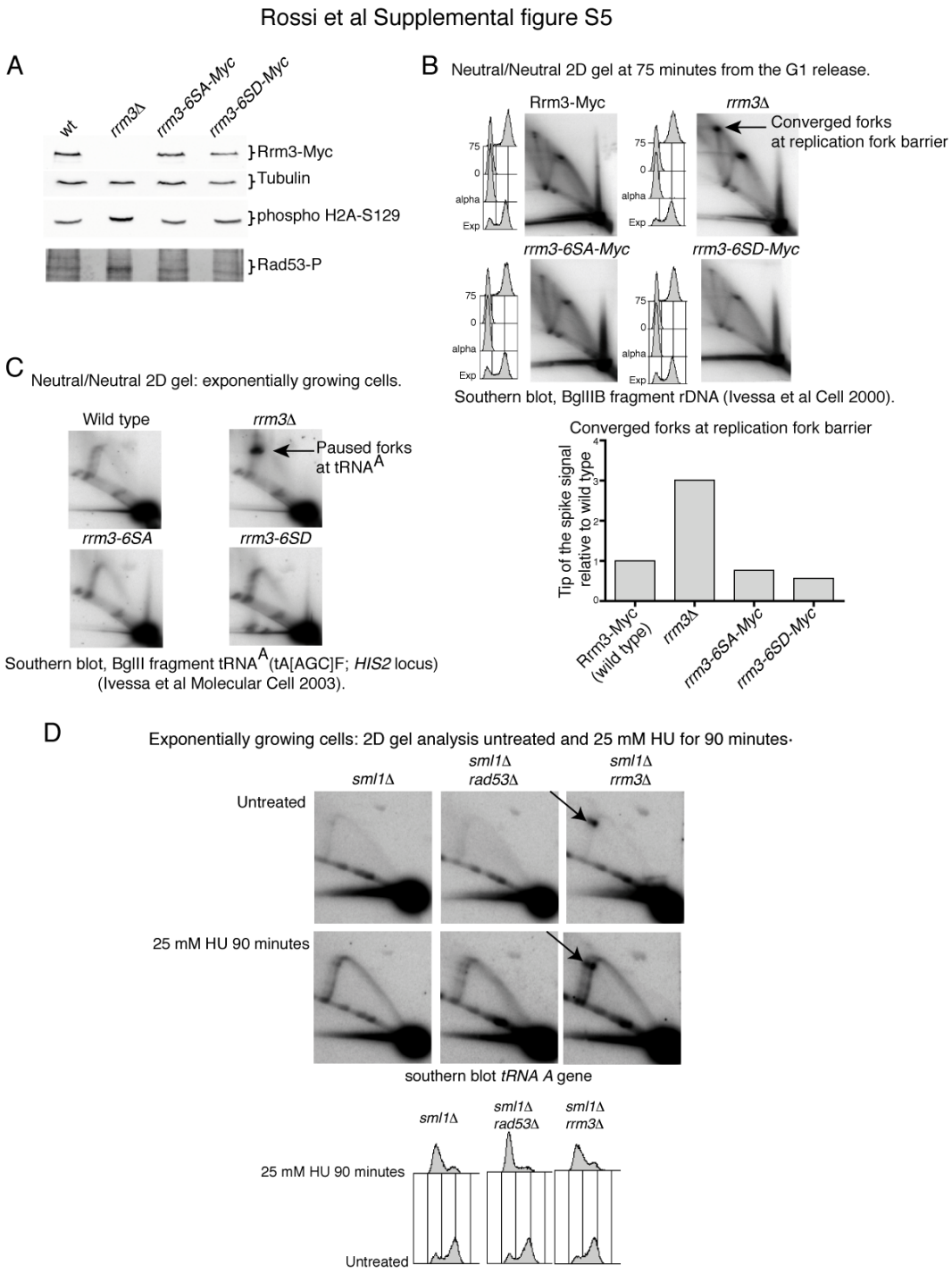

Figure S5. The *rrm3-6SA*, *rrm3-6SD*, *pif1-12A* and *pif1-12D* alleles do not influence protein levels and protein functions in unperturbed conditions, (related to Figure 5). A) The yeast strains *RRM3-13MYC* (CY11360), *rrm3Δ* (CY12484), *rrm3-6SA-13MYC* (CY12803), *rrm3-6SD-13MYC* (CY12831) carrying the indicated *RRM3* alleles have been grown to mid log phase in unperturbed conditions. Protein extracts have been prepared and separated by SDS page. Rrm3 variants, tubuline, histone H2A phosphorylation and Rad53 phosphorylation have been visualized by

western blotting using specific antibodies. **B)** DNA replication intermediates accumulating in the BglIIB fragment of the rDNA (Ivessa et al., 2000), have been visualized through neutral-neutral 2D gel electrophoresis in the yeast strains used in A at 75 minutes from the G1 release in unperturbed conditions. FACS profiles, which show the cellular DNA content during the experiments, are shown. The signals at the tip of the spike arc (corresponding to converged replication forks at the replication fork barrier in the rDNA) (Ivessa et al., 2000), have been normalized against the intensity of their corresponding monomer spots and reported into the histogram as values relative to the wild type signal. **C)** DNA replication intermediates accumulating in the BglII fragment containing the *HIS2* and the $tRNA^{A}$ tA[AGC]F coding region, have been visualized through neutral-neutral 2D gel electrophoresis in the yeast strains wild type (CY12486), *rrm3Δ* (CY12484), *rrm3-6SA*(CY12801) and *rrm3-6SD* (CY12824) grown to mid log phase in unperturbed conditions (Ivessa et al., 2003). **D) Exponentially growing wild type and *rad53Δ* cells do not accumulate DNA replication pausing signals at the *tRNA*^{A} gene even when cells are treated with 25mM of HU for 90 minutes.** CY12445, CY12443 and CY12448 strains were grown to mid log phase and DNA replication intermediates, accumulating on the BglII-*HIS2* restriction fragment containing the *tRNA*^{A} gene, have been analyzed by 2D gel electrophoresis in unperturbed conditions or after 90 minutes of treatment of exponentially growing cells with 25 mM of HU. FACS profiles, which show the cellular DNA content during the experiment, are reported. A black arrow indicates the DNA replication pausing signal induced at the *tRNA*^{A} locus by the absence of *RRM3*.

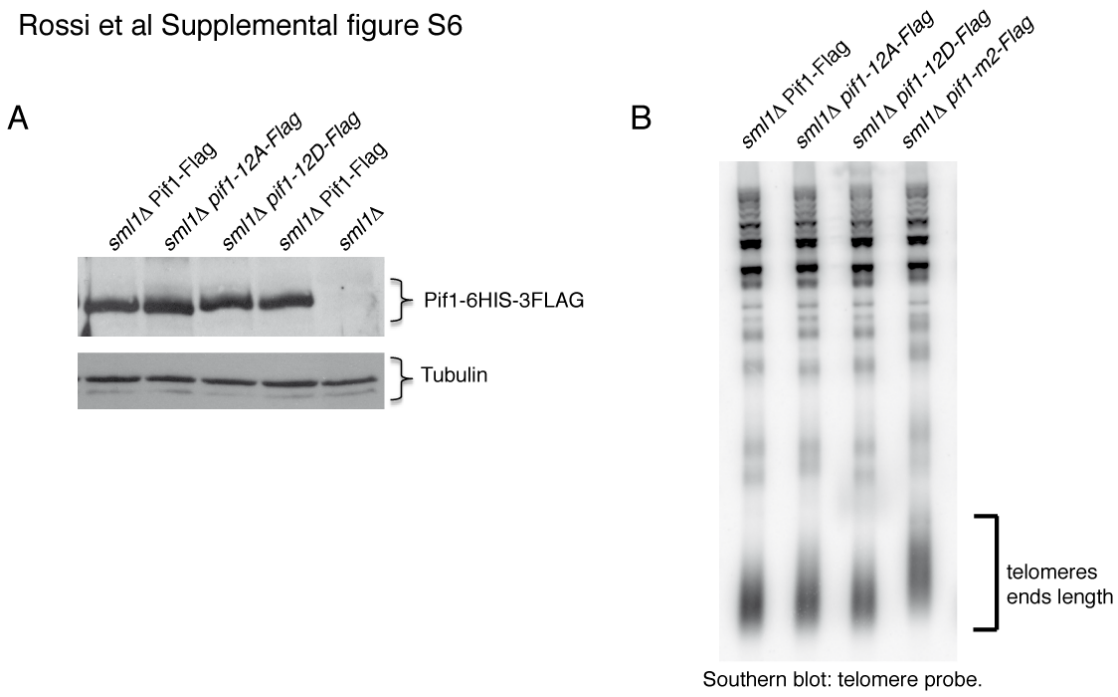

Figure S6 (related to Figure 5).

A) The following yeast strains: *sml1Δ PIF1-6HIS-3FLAG* (CY13074), *sml1Δ pif1-12A-6HIS-3FLAG* (CY13664), *sml1Δ rad53Δ pif1-12D-6HIS-3FLAG* (CY13668), *sml1Δ* (CY12445), have been grown to mid log phase in unperturbed conditions. The protein levels of Pif1-6His-3Flag, *pif1-12A*-6His-3Flag and *pif1-12D*-6His-3Flag and of the tubulin (as loading control), have been analyzed by western blotting, respectively, using anti-flag antibodies and anti tubulin antibodies. **B)** The length of the telomeres has been analyzed by southern blotting using a telomere specific probe as previously described (Longhese et al., 2000) in the yeast strains used in D and in the *sml1Δ pif1-m2-6His-3Flag* strain (CY12934), which have been grown to mid log phase in unperturbed conditions.

Rossi et al. Supplemental Figure S7

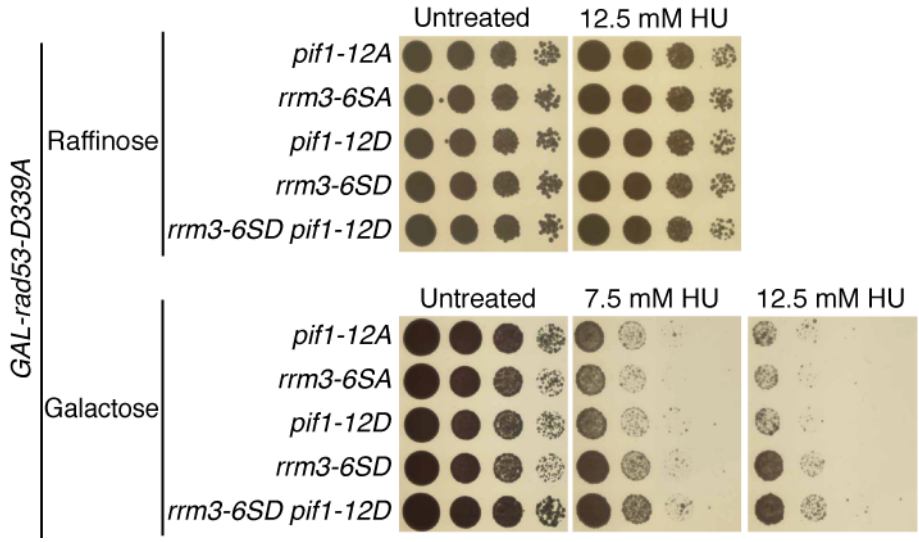

Figure S7 (related to Figure 5).

HU sensitivity has been determined by drop assay at the indicated HU dosages in YP+Raffinose or YP+Raffinose+Galactose in strains: *leu2::2X-LEU2-GAL1-rad53-D339A sml1Δ pif1-12A-6HIS-3FLAG RRM3-13MYC* (CY14011), *leu2::2X-LEU2-GAL1-rad53-D339A sml1Δ Pif1-6HIS-3FLAG rrm3-6SA-13MYC* (CY14013), *leu2::2X-LEU2-GAL1-rad53-D339A sml1Δ pif1-12D-6HIS-3FLAG RRM3-13MYC* (CY14012), *leu2::2X-LEU2-GAL1-rad53-D339A sml1Δ Pif1-6HIS-3FLAG rrm3-6SD-13MYC* (CY14014), *leu2::2X-LEU2-GAL1-rad53-D339A sml1Δ pif1-12D-6HIS-3FLAG rrm3-6SD-13MYC* (CY14015).

Supplemental experimental procedures

Cell were grown in YPD (2% glucose), arrested in alpha factor (4 µg/ml) at 28°C for 2 hours and released with/without HU (25 mM or 150 mM). ChIP on chip experiments were performed and protein-DNA binding profiles generated as described (Bermejo et al., 2009a; Bermejo et al., 2009b) based on the affymetrix platform. PCR amplification steps in our ChIP on chip analysis were carried out under non saturating conditions and the amounts of DNA used to hybridize the affymetrix chips were normalized. The significance of the overlaps between the protein binding clusters and protein binding clusters and BrdU clusters, was evaluated by confrontation against a null hypothesis model generated with a Montecarlo-like simulation, as described (Bermejo et al., 2009a; Bermejo et al., 2009b). The average

binding signals of the indicated proteins at 141 early *ARSs* (Figure 1C), were plotted using the sitepro function in CEAS (Cis-regulatory Element Annotation System) (Shin et al., 2009). We set 50 nt as the profiling resolution and 12,000 nt as the size of flanking regions from the center of each *ARS* (Shin et al., 2009). ssDNA-BrdU IP on chip experiments and profiles has been conducted/generated as described (Katou et al., 2003). Quantitative ChIP-qPCRs using the oligos 305L3F (CCATGACTTTGGCACATCAG) and 305L3R (CGCTGCCTCCTTAGTAATCG) for the strains (CY11360, CY12425, CY12927, CY12698) and the oligos 305L8F (TCAAAGCAGATGCCATGAAC) and 305L8R (CTGTTTGCACGAAGGAATCA) for the strains (CY13074, CY13073, CY13284, CY13282) (see figure 1A-B-D), have been performed as described (Alzu et al., 2012). 2D gel electrophoresis has been conducted on genomic DNA prepared with the C-tab method after sodium azide fixation (40 minutes on ice 0.1% final concentration) and *in-vivo* psoralen cross linking as described (Liberi et al., 2006). PFGE electrophoresis analysis using Amersham gene navigator system has been performed as described (Giannattasio et al., 2010) on sodium azide-treated cellular pellets using the following program: 165V, 23 hours of run with 30 seconds pulses step wise. Phospho-tag gels (7.5%-10% with ratio acrylamide/bis-acrylamide of 75:1 and 40 μM of P-tag reagent) has been prepared according to manufacturer instructions (Kinoshita et al., 2006). Analysis of replication forks by trasmission electron microscopy has been performed as described (Neelsen et al., 2014). All the strains used in this study are listed in Table S1 and are W303 derivatives with the wild type *RAD5* locus. The *rrm3* and *pif1* alleles have been generated using the "delitto perfetto" strategy (Storici and Resnick, 2006). Mutant alleles expressing fusion proteins with different tags have been generated by one step replacement systems using different template plasmids as described (Longtine et al., 1998).

Supplemental references

Alzu, A., Bermejo, R., Begnis, M., Lucca, C., Piccini, D., Carotenuto, W., Saponaro, M., Brambati, A., Cocito, A., Foiani, M., *et al.* (2012). Senataxin Associates with Replication Forks to Protect Fork Integrity across RNA-Polymerase-II-Transcribed Genes. Cell *151*, 835-846.

Bermejo, R., Capra, T., Gonzalez-Huici, V., Fachinetti, D., Cocito, A., Natoli, G., Katou, Y., Mori, H., Kurokawa, K., Shirahige, K., *et al.* (2009a). Genome-organizing

factors Top2 and Hmo1 prevent chromosome fragility at sites of S phase transcription. Cell *138*, 870-884.
Bermejo, R., Katou, Y.M., Shirahige, K., and Foiani, M. (2009b). ChIP-on-chip analysis of DNA topoisomerases. Methods in molecular biology *582*, 103-118.
Giannattasio, M., Follonier, C., Tourriere, H., Puddu, F., Lazzaro, F., Pasero, P., Lopes, M., Plevani, P., and Muzi-Falconi, M. (2010). Exo1 competes with repair synthesis, converts NER intermediates to long ssDNA gaps, and promotes checkpoint activation. Mol Cell *40*, 50-62.
Ivessa, A.S., Lenzmeier, B.A., Bessler, J.B., Goudsouzian, L.K., Schnakenberg, S.L., and Zakian, V.A. (2003). The Saccharomyces cerevisiae helicase Rrm3p facilitates replication past nonhistone protein-DNA complexes. Mol Cell *12*, 1525-1536.
Ivessa, A.S., Zhou, J.Q., and Zakian, V.A. (2000). The Saccharomyces Pif1p DNA helicase and the highly related Rrm3p have opposite effects on replication fork progression in ribosomal DNA. Cell *100*, 479-489.
Kinoshita, E., Kinoshita-Kikuta, E., Takiyama, K., and Koike, T. (2006). Phosphate-binding tag, a new tool to visualize phosphorylated proteins. Molecular & cellular proteomics : MCP *5*, 749-757.
Liberi, G., Cotta-Ramusino, C., Lopes, M., Sogo, J., Conti, C., Bensimon, A., and Foiani, M. (2006). Methods to study replication fork collapse in budding yeast. Methods in enzymology *409*, 442-462.
Longhese, M.P., Paciotti, V., Neecke, H., and Lucchini, G. (2000). Checkpoint proteins influence telomeric silencing and length maintenance in budding yeast. Genetics *155*, 1577-1591.
Longtine, M.S., McKenzie, A., 3rd, Demarini, D.J., Shah, N.G., Wach, A., Brachat, A., Philippsen, P., and Pringle, J.R. (1998). Additional modules for versatile and economical PCR-based gene deletion and modification in Saccharomyces cerevisiae. Yeast *14*, 953-961.
Neelsen, K.J., Chaudhuri, A.R., Follonier, C., Herrador, R., and Lopes, M. (2014). Visualization and interpretation of eukaryotic DNA replication intermediates in vivo by electron microscopy. Methods in molecular biology *1094*, 177-208.
Shin, H., Liu, T., Manrai, A.K., and Liu, X.S. (2009). CEAS: cis-regulatory element annotation system. Bioinformatics *25*, 2605-2606.
Storici, F., and Resnick, M.A. (2006). The delitto perfetto approach to in vivo site-directed mutagenesis and chromosome rearrangements with synthetic oligonucleotides in yeast. Methods in enzymology *409*, 329-345.